Vapor-liquid equilibrium data for the carbon dioxide and carbon monoxide (CO_2 + CO) system at the temperatures 253, 273, 283 and 298 K and pressures up to 13 MPa

Snorre Foss Westman[a,*], Anders Austegard[a], H. G. Jacob Stang[a], Sigurd W. Løvseth[a,**]

[a] *SINTEF Energy Research, P.O. Box 4761 Torgarden, NO-7465 Trondheim, Norway*

Abstract

Vapor-liquid equilibrium measurements for the binary system CO_2+CO are reported at 253, 273, 283 and 298 K, with estimated standard uncertainties of maximum 9 mK in temperature, maximum 3 kPa in pressure, and maximum 0.001 in the mole fractions of the phases in the mixture critical regions, and 0.0003 in the mole fractions outside the critical regions. These measurements are compared with existing data. Although some data exist, there are little trustworthy literature data around critical conditions, and the measurements in the present work indicate a need to revise the parameters of existing models. The data in the present work have significantly less scatter than most of the literature data, and range from the vapor pressure of pure CO_2 to close to the mixture critical point pressure at all four temperatures. With the measurements in the present work, the data situation for the CO_2+CO system is improved, enabling development of better equations of state for the system. A scaling law model is fitted to the critical region data of each isotherm, and high accuracy estimates for the critical composition and pressure are found. The Peng-Robinson EOS with the alpha correction by Mathias and Copeman, the mixing rules by Wong and Sandler, and the NRTL excess Gibbs energy model is fitted to the data in the present work.

Keywords:
vapor-liquid equilibrium, experimental, measurements, carbon dioxide, carbon monoxide, CO_2 capture and storage

1. Introduction

According to leading authorities regarding the future of the global energy system, like IEA [3], large amounts of CO_2 have to be captured, transported and stored in order to facilitate a cost-effective transition to sustainable energy production and consumption needed to avoid excessive anthropogenic climate change. Hence, there has been a renewed interest in the properties of CO_2 with relevant impurities. As discussed in Refs. [4, 5, 6, 7], there are great need for data on these systems as there are still many critical knowledge gaps, and even small amount of impurities may drastically alter the properties of CO_2-rich mixtures [7, 8]. For instance, cricondenbar may increase and density change compared to pure CO_2, which could lead to increased compressor work and costs [9, 8]. Hence, for the realization of future robust and cost-efficient processes for CO_2 capture, transport, and capture (CCS) processes, precise fluid models built on high-quality data must be developed.

Similar to what was noted in our previous work [2] for CO_2+O_2, the modeling of the thermodynamics of CO_2+CO have been restricted by the lack of high quality data and lack of consistency between the available data sets, for instance during the development of the EOS-CG equation of state (EOS) [5, 6]. CO is produced in oxygen-lean processes and can in CCS be found in captured CO_2 from e.g. refineries and pre-combustion processes, in concentrations up to 0.2% [10]. A large part of existing literature data is rather old, and there are significant gaps in the critical region and at higher temperatures [4, 5, 6, 7].

In the work presented here, new VLE data were experimentally produced for the CO_2+CO system. Four isotherms at 253.15, 273.16, 283.30 and 298.16 K have been measured, spanning the upper part of the VLE temperature region of this binary system. The pressure of the new data points ranges from 1.97 to 12.6 MPa. The new data points cover gaps and regions of inconsistencies in available literature data, for instance close to critical conditions and at the technological important temperatures above 273 K. The measurements are compared with existing data and EOSes Furthermore, a cubic EOS is fitted to the data at each isotherm, and the parameters of the models are regressed such that the EOS can be used over the full temperature range of the measurements.

The measurements of the current work were performed using a fit-to-purpose setup [11] constructed in order to perform precise phase equilibria measurements on mixtures and at conditions expected in CCS [7, 12]. The setup was constructed as part of the BIGCCS/CO_2Mix project [8, 13]. In addition to the new data on CO_2+CO reported in the current paper, this facility has also been used to measure phase equilibrium data on CO_2+N_2 [1], CO_2+O_2 [2], CO_2+CH_4 [14]

*Corresponding author.
**Corresponding author.
Email addresses: snorre.foss.westman@sintef.no (Snorre Foss Westman), sigurd.w.lovseth@sintef.no (Sigurd W. Løvseth)

This is the accepted version of an article published in Fluid Phase Equilibria
https://doi.org/10.1016/j.fluid.2018.05.006

and CO_2+Ar [15]. As in the previous work, new data are reported in accordance with journal and IUPAC Guidelines Chirico et al. [16], including uncertainty estimates according to a detailed analysis [17, 1, 2].

Section 2 of this paper presents the experimental facility and methods used, and Section 3 presents the uncertainty analysis pertaining to the new data. The new data are provided and analyzed in Sections 4 and 5. The analysis includes model fitting. Conclusions of the work are provided in Section 6.

2. Experimental apparatus

2.1. Description of setup

The apparatus used for the VLE measurements in the present work was described and validated in Ref. [1], and a summary was presented in Ref. [2]. The measurements were performed using the isothermal analytical method with a variable volume cell (100 cm^3), where samples of the two coexisting phases were taken at constant equilibrium temperature and pressure. To compensate for the pressure drop caused by sampling, a bellows was expanded upon each sampling, lowering the volume of the cell. The temperature of the cell was measured using two Fluke model 5686 standard platinum resistance thermometers (SPRTs), placed in the flanges of the cell. The pressure of the cell was measured indirectly using an array of 4 absolute pressure sensors, Keller type PAA-33X, with a differential pressure sensor, Rosemount type 3051 with 1199 diaphragm. For details regarding the measurement chain, please refer to Ref. [1]. Almost all aspects of the experimental setup were unchanged compared to in Ref. [2], and only the differences will be presented here. A diagram of the cell and apparatus is shown in Fig. 1.

2.2. Calibration

The calibration of the temperature and pressure sensors was performed in-house. The temperature sensors were calibrated against fixed point cells according to the International Temperature Scale of 1990 (ITS-90). The pressure sensors were calibrated against a dead weight tester calibrated recently. In addition, the use of two temperature sensors and multiple pressure sensors would have exposed sudden changes in any of the sensors. Details concerning the estimated temperature and pressure measurement uncertainties are given in Section 3.2 below, and discussed in detail in Ref. [1].

The gas chromatograph (GC) was calibrated against reference gas mixtures prepared in-house using our custom built apparatus for gravimetric preparation of mixtures. Details about the calibration gas mixtures and the calibration can be found in Section 3.3 below. Both in the VLE experiments and in preparing the reference gas mixtures the same source gases of pure CO_2 and CO were used. The manufacturer's specification of the purities of these source gases are given in Table 1. No additional analysis of the specified purities of these gases was performed.

2.3. Experimental procedures

The experimental procedures used in Ref. [2] were also followed in the present work. This can be summarized as stirring the cell contents to equilibrium (stable pressure and temperature), visual confirmation of the presence of the phase boundary, settling of the phases after the stirrer stopped, and sampling of the liquid and vapor phases after flushing the sampling capillaries. Normally, 7 samples were taken from each phase. For further details regarding the experimental procedure and the duration and criteria of each step, please see Section 2.3 in Ref. [2].

As the experiments involved carbon monoxide, which is toxic by inhalation, additional HSE precautions were carried out. The experimental rig was designed with safety in mind, and measures to avoid and contain leaks of gas components into the surrounding air were in place from before. In addition to the standard gas sensors and alarms, the operators of the experimental rig used supplied air respirators to ensure that they were not exposed to carbon monoxide through inhalation in the event of a unexpected leak. To the best of our knowledge, there did not exist air respirators that could filter carbon monoxide from the air surrounding the operator, and it was therefore essential that the air respirator was supplied with fresh, filtered breathing-quality air through airhose from outside the area where carbon monoxide could be present.

3. Uncertainty analysis

3.1. Definitions

The terms and definitions in the "GUM" [17] are used in the uncertainty analysis. The uncertainties are evaluated as standard uncertainties, with symbol $u(y)$, where y is the estimate of the measurand Y. The propagation of the standard uncertainties in input quantities X_i into a final calculated value Y is described by the combined standard uncertainty, with symbol $u_c(y)$.

3.2. Pressure and temperature

A thorough analysis of the uncertainty of the pressure and temperature measurements was performed in Ref. [1], where VLE measurements of the CO_2+N_2 system were performed. The same methodology was used for the measurements in the present work, the only difference being that the density used in the hydrostatic pressure calculations was calculated using EOS-CG [5, 6] for CO_2+CO instead of CO_2+N_2. Only the resulting uncertainty estimates are given here. The details of the uncertainty analysis methodology can be found in Ref. [1].

The uncertainty components contributing to the standard uncertainty for the measured pressure p at VLE were summarized in Table 2 in Ref. [2], and the resulting standard uncertainties in the pressure measurements are shown in Tables 5 and 6. The only change to the uncertainty components in Table 2 in Ref. [2] is the standard uncertainty of the vapor density used in the hydrostatic pressure calculation, $u(\rho_1)$,

This is the accepted version of an article published in Fluid Phase Equilibria
https://doi.org/10.1016/j.fluid.2018.05.006

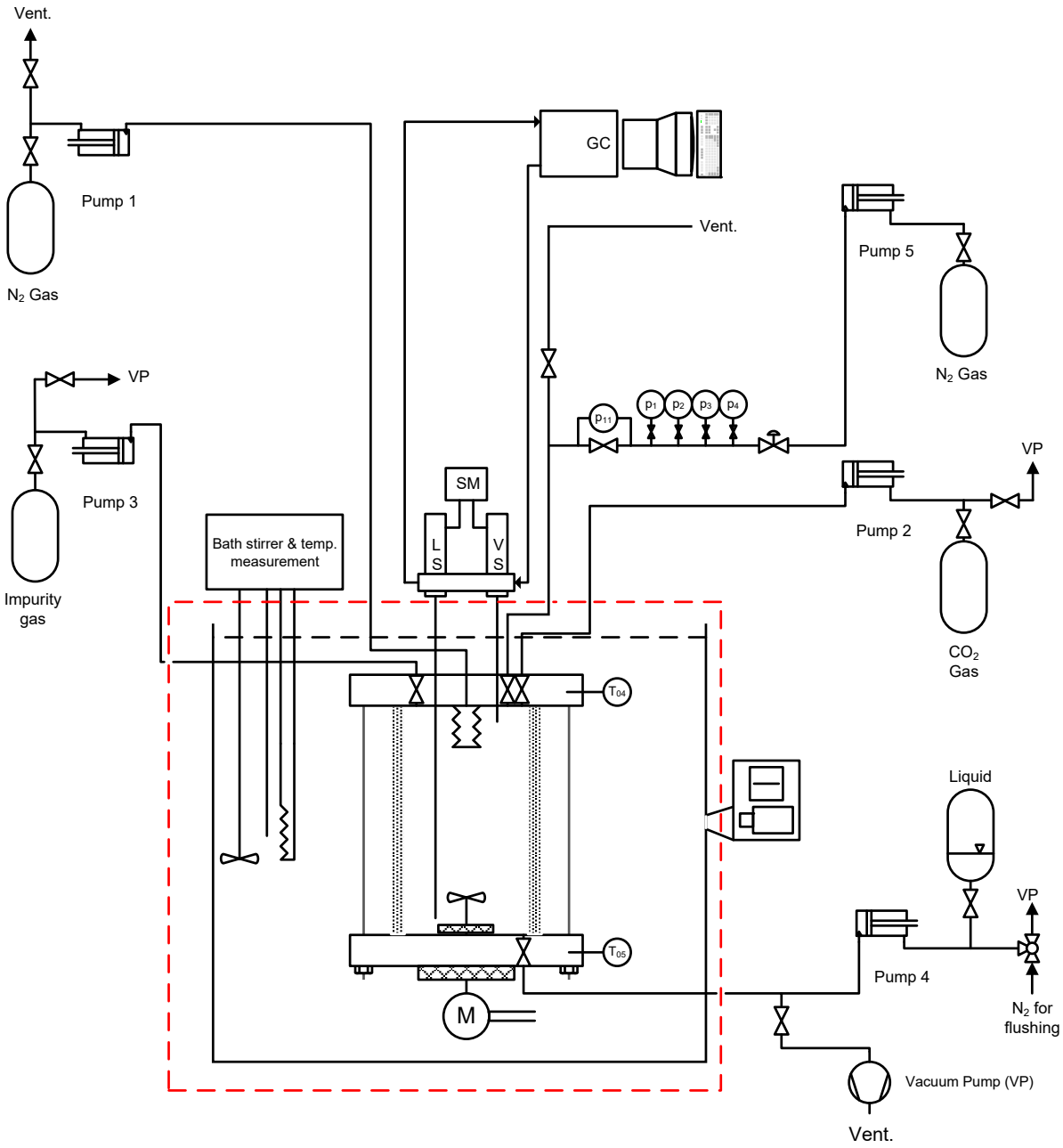

Fig. 1. Figure from [1, 2]: Principal diagram of cell and ancillary apparatus. LS,VS: Liquid and vapor phase Rolsi^{TM} samplers, respectively. SM: Rolsi^{TM} controller. M: Gear for rotating permanent magnet below cell, which rotates stirrer inside cell. Gear connected to electric motor outside bath. T_{04}: Top flange SPRT. T_{05}: Bottom flange SPRT. Absolute pressure sensors, p_i, where i =1,2,3,4, with full scales 1, 3, 10 and 20 MPa, respectively. Differential pressure sensor p_{11}.

This is the accepted version of an article published in Fluid Phase Equilibria
https://doi.org/10.1016/j.fluid.2018.05.006

which was estimated to be $1 \cdot 10^{-2} \cdot \rho_1$ for of CO_2+CO in EOS-CG [5, 6]. Similarly, Table 3 in Ref. [2] and Tables 5 and 6 show the contributors to and the resulting standard uncertainty in the measured temperatures T.

As seen from Tables 5 and 6, the standard uncertainty in the pressure was estimated to be below 0.03% of the measured pressure. Similarly, the standard uncertainty in the temperature was estimated to be below 9 mK, and the variation in temperature had been less than 1 mK for each data point.

The measurements of the CO_2 vapor pressure at each temperature provided an additional check of the temperature and pressure sensors, when compared with values calculated with the Span-Wagner EOS for CO_2. With reference to Tables 5 and 6, the measured CO_2 vapor pressures were consistent with the calculated values when the expanded uncertainty was counted for both in the measurements and the calculated values from the EOS.

3.3. Composition

The VLE phase composition analysis and uncertainty estimation were performed in the same manner as in Refs. [1, 2], with the methodology applied to CO_2+CO samples instead of CO_2+N_2/O_2. A summary will be provided here, with reference to Refs. [1, 2] for further details.

The composition analysis was performed using the same GC as in Refs. [1, 2], with its calibration performed using gravimetrically prepared reference gas mixtures using a custom-built rig in our laboratories [18].

For the measurement method utilized in the present work and in Refs. [1, 2], it could be stated that the composition uncertainty stemmed from a range of sources, including the impurities of the gases used to prepare the reference mixtures, the uncertainty in the molar masses, inaccuracies in the weighed masses, adsorption, chemical reactions, repeatability / uncertainties of the sampling and GC analysis, and finally the consistency between the GC calibration function and data. The analysis of these contributing factors are given below.

3.3.1. Source gas composition and molar mass

Following the methodology in Refs. [2, 1], the composition and the corresponding uncertainty of a gravimetrically prepared gas mixture can be stated to be results of both the purity and the molar mass of the source gases used for the mixture. According to Refs. [19, 20], the molar masses of monoatomic carbon C, monoatomic oxygen O in commercial tank gas CO_2 and monoatomic carbon C, monoatomic oxygen in commercial tank gas CO generally lie within ranges of width 0.6, 0.15, 0.2 and 0.3 mg mol^{-1}, respectively. Based on this, the molar masses of CO_2 and CO, M_{CO_2} and M_{CO} respectively, were calculated with the corresponding uncertainty estimates shown in Table 2.

Table 2
Molar masses of atomic elements and compounds with uncertainties [19, 20], calculated considering the impurities in the source gases in Table 1.

Component i	M_i	$u(M_i)$	Unit
C[a]	0.0120108	0.0000003	kg mol^{-1}
O[a]	0.01599938	0.00000007	kg mol^{-1}
C[b]	0.0120108	0.0000001	kg mol^{-1}
O[b]	0.01599920	0.00000015	kg mol^{-1}
CO_2	0.0440096	0.0000003	kg mol^{-1}
CO	0.0280100	0.0000002	kg mol^{-1}
CO_2+imp	0.0440095		kg mol^{-1}
CO+imp	0.0280098		kg mol^{-1}
CO_2,eff	0.0440097		kg mol^{-1}
CO,eff	0.0280102		kg mol^{-1}

[a] In CO_2 molecule
[b] In CO molecule

The minimum certified purities of the CO_2 and CO source gases used to prepare the reference gas mixtures are given in Table 1, together with the manufacturers' specifications of the maximum content of certain impurities. Since the source gases were not entirely pure, estimates for the molar masses of the source gases, M_{CO_2+imp} and M_{CO+imp}, should account for the impurities present, following the procedure used in Ref. [1].

M_{CO_2+imp} and M_{CO+imp} were calculated based on the impurity specifications stated in Table 1. The molar mass of each impurity was calculated using data from Wieser et al. [20], assuming methane CH_4 for the hydrocarbon impurity fraction. The molar masses of the source gases, M_{CO_2+imp} and M_{CO+imp}, together with the effective molar masses of the source gases excluding the impurities, $M_{CO_2,eff}$ and $M_{CO,eff}$, are shown in Table 2.

3.3.2. Carbon monoxide chemistry

CO is under certain conditions a reactive component. For instance, it is known that CO may disproportionate into CO_2 and solid C through the so-called Boudouard reaction. Below about 900-1100 K, the chemical equilibrium of this reaction favor formation of CO_2 and C. However, the activation energy is high, and hence the CO is stable at the temperatures and pressures of this work unless passed over a catalyst or e.g. optically excited [21]. Further, it is well established that

Table 1
Chemical samples used.

Chemical name	CASRN	Source	Initial mole fraction purity	Purification method	Final mole fraction purity	Analysis method
Carbon dioxide[a]	124-38-9	AGA (from Linde)	0.999 993	None	0.999 993	None
Carbon monoxide[b]	630-08-0	AGA (from Linde)	0.999 97	None	0.999 97	None
Helium[c]	7440-59-7	AGA (from Linde)	0.999 999	None	0.999 999	None

[a] Maximum specified impurity content by volume was less than 1 ppm H_2O, 2 ppm O_2, 3 ppm N_2, 1 ppm hydrocarbons C_nH_m and 0.5 ppm CO.
[b] Maximum specified impurity content by volume was less than 5 ppm H_2O, 5 ppm O_2, 20 ppm N_2, 2 ppm hydrocarbons C_nH_m, 30 ppm H_2 and 15 ppm Ar.
[c] GC carrier gas.

This is the accepted version of an article published in Fluid Phase Equilibria
https://doi.org/10.1016/j.fluid.2018.05.006

Table 3
CO_2 + CO reference gas mixtures

$y_{CO_2,cal}$	$u(y_{CO_2,cal}, m)$	$u(y_{CO_2,cal}, M_{eff})$	$u(y_{CO_2,cal}, ads.)$	$u_c(y_{CO_2,cal})$
0.293674	$1.3 \cdot 10^{-6}$	$7.1 \cdot 10^{-6}$	$14.4 \cdot 10^{-6}$	$16.1 \cdot 10^{-6}$
0.498553	$1.1 \cdot 10^{-6}$	$4.2 \cdot 10^{-6}$	$6.0 \cdot 10^{-6}$	$7.4 \cdot 10^{-6}$
0.704087	$2.2 \cdot 10^{-6}$	$4.5 \cdot 10^{-6}$	$2.5 \cdot 10^{-6}$	$5.6 \cdot 10^{-6}$
0.896948	$2.5 \cdot 10^{-6}$	$7.1 \cdot 10^{-6}$	$0.7 \cdot 10^{-6}$	$7.5 \cdot 10^{-6}$

CO may form volatile carbonyls with metals such as cobalt, iron, and nickel [22, 23]. Apart from depleting the CO, formation of carbonyls also would be an HSE hazard as they are extremely poisonous and a corrosion problem. Carbonyls do not easily form with aluminium, titanium, or high-chrome steel, and is also reduced by suitable coatings [24, 25].

Hence, high purity CO, as specified in Table 1, require careful selection of the materials used for storing and transportation, to lower the possibility for this reaction to occur to a significant degree. The production of metal carbonyls is a relatively slow process, and hence the cylinders used to store the pure CO and the CO+CO_2 reference mixtures are probably of highest importance. The pure CO obtained from AGA/Linde was delivered in aluminum cylinders (Luxfer Gas Cylinders Ltd.). The cylinders used to prepare the reference gas mixtures for CO_2+CO, including the reference cylinder used to reduce the effect of varying buoyancy, were Luxfer aluminum alloy cylinders provided by Scott Specialty Gases. To comply with exposure to CO, the internal walls of the cylinders had gone through a proprietary inerting treatment (Scott Specialty Gases ACULIFE® III), where a coating was applied through chemical vapor deposition to enhance the stability of reactive gas and liquid mixtures. This treatment also increased the adsorption resistance of the gas cylinders.

Further, the flow path for the reference gases and pure CO leading from the gas cylinders used high chromium steeel (Hastelloy C-276) coated with Silconert® passivation layer. The equilibrium cell itself was made of titanium and sapphire. No indications of carbonyls were found in the gas chromatograms of the samples extracted from the cell.

3.3.3. Gravimetric preparation of reference gas mixtures

As in Ref. [2], the methodology of gravimetric preparation of the reference gas mixtures and the uncertainty estimation given in Refs. [1, 18] was used in the present work, with only a modification of the calculation of the adsorption uncertainty $u(y_{CO_2,cal}, ads.)$. This modification will be discussed in Section 3.3.4. Details regarding the methodology and the other uncertainty terms are given in Appendix A.3.4 in Ref. [1].

Four CO_2+CO reference gas mixtures were made, spanning in CO_2 mole fractions $y_{CO_2,cal}$ from 0.29 to 0.90. An overview of the mixtures is given in Table 3.

3.3.4. Composition calibration procedure and estimated composition uncertainty

The calibration of the GC was performed as described in Ref. [2] and in Appendix A.3.1 in Ref. [1], where thorough flushing of the gas lines and cell with the reference gas mixture lowered the risk of adsorption of the gas onto the contact surfaces changing the composition significantly from that in the gas cylinders. Samples of varying sizes were withdrawn from the cell at different pressures between 5 and 10 MPa. These samples formed the calibration basis for the composition analysis, establishing a relation between the CO_2 mole fractions of the reference gas mixtures and the GC detector response.

The uncertainty contribution from the reference mixture uncertainty reaching the GC, $u_c(y_{CO_2,cal})$, was estimated using Eq. (1) in Ref. [2]. The uncertainty estimates are provided in Table 3, where $u(y_{CO_2,cal}, m)$ is the uncertainty in mole fraction due to the gravimetric preparation, $u(y_{CO_2,cal}, M_{eff})$ is the uncertainty in mole fraction due to uncertainty in molar mass, and $u(y_{CO_2,cal}, ads.)$ is the uncertainty in mole fraction due to the assumed stronger tendency for CO_2 than CO to adsorb at the walls of the VLE cell and gas cylinders. The latter uncertainty was calculated from:

$$u(y_{CO_2,cal}, ads.) \approx \frac{1}{2} \cdot \Delta y_{CO_2,maximum\ adsorption}, \tag{1}$$

where

$$\Delta y_{CO_2,maximum\ adsorption} \approx \tag{2}$$

$$\frac{n_{CO,cyl.} \cdot \Delta n_{CO_2,max.ads.cyl.}}{n_{CO_2,cyl.} \cdot \left(n_{CO_2,cyl.} + n_{CO,cyl.}\right)} + \frac{n_{CO,cell} \cdot \Delta n_{CO_2,max.ads.cell}}{n_{CO_2,cell} \cdot \left(n_{CO_2,cell} + n_{CO,cell}\right)}, \tag{3}$$

with $\Delta n_{CO_2,max.ads.cyl.}$, $\Delta n_{CO_2,max.ads.cell}$ and the mole values in the cell $n_{CO_2,cell}$ and $n_{CO,cell}$ were calculated as in Appendix A.3.4 in Ref. [1].

As seen in Table 3, the uncertainty contribution from the molar mass of CO caused $u(y_{CO_2,cal}, M_{eff})$ to dominate the combined standard uncertainty of the CO_2 mole fraction $u_c(y_{CO_2,cal})$ for the gas mixtures with the highest CO_2-content. For the mixtures with the lowest CO_2-content, the uncertainty contribution from the adsorption of CO_2 dominated, which can be explained by the larger impact of changes in moles of CO_2 relative to moles of CO_2 in the gas cylinder and in the cell.

3.3.5. GC integration and calibration function

The GC column, method and detector used for CO_2+N_2 and CO_2+O_2 samples in Refs. [1, 2] were utilized on CO_2+CO samples in the present work, with helium as the GC carrier gas. This setup gave just as good separation of the CO_2 and CO peaks in the GC chromatogram as for the previous systems. The areas under the CO_2 and CO peaks in the chromatogram, denoted A_{CO_2} and A_{CO}, were obtained for each sample by numerical integration.

As for the CO_2+O_2 system in Ref. [2], the GC thermal conductivity detector (TCD) response was nonlinear with respect to the number of moles of CO_2 and CO passing through the detector. The following model, consisting of both linear and nonlinear terms, described adequately the relation between moles of each component in the sample to the area of

This is the accepted version of an article published in Fluid Phase Equilibria
https://doi.org/10.1016/j.fluid.2018.05.006

Table 4
Fitted parameters of the $\bar{\hat{y}}_{CO_2,cal}$ model and standard uncertainty of composition analysis $\bar{u}_c(x_{CO_2})$ and $\bar{u}_c(y_{CO_2})$.

Variable	Liquid	Vapor
c_1	1.041 801	0.902 973
c_2	1.5	1.5
c_3	1.146 512	1.145 374
c_4	2.330 930	2.091 908
c_5	1.5	1.5
$\bar{u}_c(z_{CO_2}) \approx RMSE = s(e)$	$3.2 \cdot 10^{-4}$	$2.6 \cdot 10^{-4}$
n data points used in fit	16	21
p fitted parameters	3	3
ν degrees of freedom	13	18
SSE	$1.24 \cdot 10^{-6}$	$1.14 \cdot 10^{-6}$

each component:

$$\hat{n}_{CO_2} \cdot k = A_{CO_2} + 10^{-3} \cdot c_1 \cdot (A_{CO_2})^{c_2} , \quad (4)$$

$$\hat{n}_{CO} \cdot k = c_3 \cdot A_{CO} + 10^{-3} \cdot c_4 \cdot (A_{CO})^{c_5} , \quad (5)$$

$$\hat{y}_{CO_2,cal} = \frac{\hat{n}_{CO_2}}{\hat{n}_{CO_2} + \hat{n}_{CO}} , \quad (6)$$

where $\hat{y}_{CO_2,cal}$ is the estimator of the CO_2 mole fraction of a reference gas mixture sample given the areas for that sample, and k is an unknown factor relating the areas to the number of moles.

The parameters c_i were fitted by performing a nonlinear least squares minimization of the objective function $S = \sum_{i=1}^{n} (y_{i,CO_2,cal} - \hat{y}_{i,CO_2,cal})^2$, where $y_{CO_2,cal}$ is the actual reference mixture mole fractions given in Table 3. The parameters were fitted separately against the calibration data taken using the liquid phase and vapor phase sampler, giving one set of model parameters for each sampler. The motivation for this was the realization that there was a difference in the flow rate of the samples taken from the two samplers, causing wider and lower peaks in the samples taken using the vapor phase sampler. Since the detector response was nonlinear, this resulted in different area fractions between the samplers.

When including the parameters c_2 and c_5 in the regression, the confidence intervals of the fitted parameters indicated that some of the parameters were not significant. Consequently, the parameters c_2 and c_5 were set constant to 1.5, and c_1, c_3 and c_5 were fitted, yielding small confidence interval estimates of the parameters, with lower SSE than when c_2 and c_5 were also fitted. The resulting parameter estimates are given in Table 4.

The deviations between the reference gas mixture CO_2 mole fractions and the model predictions, $e = y_{CO_2,cal} - \bar{\hat{y}}_{CO_2,cal}$, as shown in Fig. 2, should be randomly scattered around zero over the composition range. It was difficult to determine if this was the case, especially with the reference mixture with the highest CO_2 content, where there seems to be an offset. This could indicate an inappropriate model structure, an error in the reference gas mole fraction $y_{CO_2,cal}$, or an error in the procedure execution when the calibration samples were taken.

An unbiased estimator of the standard error s for a linear regression is given by Eq. (7), expressed in terms of the mean

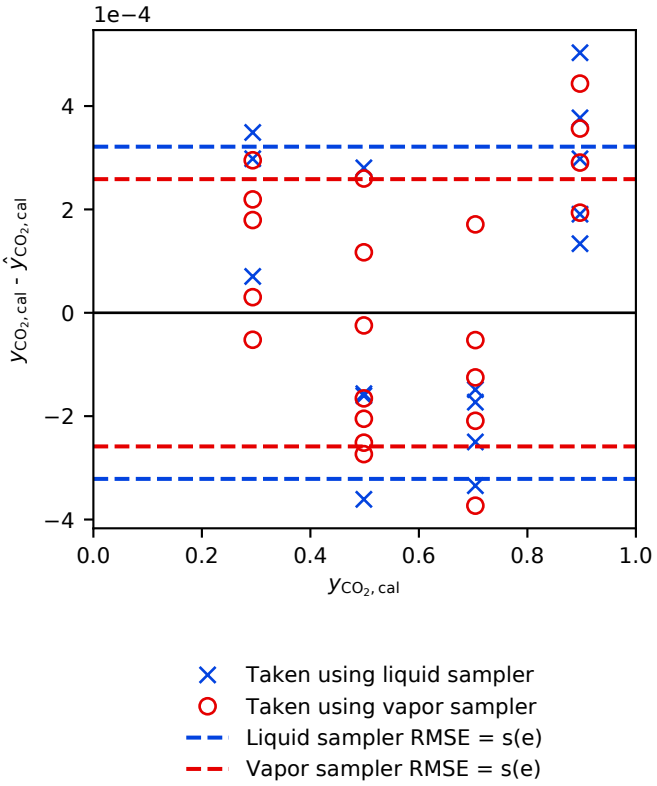

Fig. 2. Composition calibration: Error between actual compositions in Table 3 and composition model in Eq. (6), given as $y_{CO_2,cal} - \hat{y}_{CO_2,cal}$ versus $y_{CO_2,cal}$. Composition analysis uncertainty $u(x_{CO_2})$ and $u(y_{CO_2})$ assumed equal to $s(e)$ for liquid and vapor calibrations from Table 4.

This is the accepted version of an article published in Fluid Phase Equilibria
https://doi.org/10.1016/j.fluid.2018.05.006

square error MSE, the sum of squared errors of prediction SSE, the degrees of freedom v, number of data points used in the fit n and number of fitted parameters p [26].

$$s^2(e) = MSE = \frac{SSE}{v} = \frac{SSE}{n-p} = \frac{\sum_{i=1}^{n} e^2}{n-p} = \frac{\sum_{i=1}^{n} (y_i - \hat{y}_i)^2}{n-p} \tag{7}$$

However, as the model in Eq. (6) is nonlinear in the parameters, the estimator s will likely be biased [26].

It was assumed that the standard uncertainty of the CO_2 mole fraction of samples taken during VLE measurements, $\bar{u}_c(x_{CO_2})$ and $\bar{u}_c(y_{CO_2})$, was estimated by $s(e)$ for respectively the liquid and vapor sampler calibrations, because $s(e)$ was 20-45 times larger than the standard uncertainties in the mole fractions of the reference mixtures, $u_c(y_{CO_2,cal})$, provided in Table 2. To assume this behavior for the VLE mole fraction uncertainty over the whole composition range could be incorrect, considering the possible bias in $s(e)$ and the larger deviation e at the highest CO_2 mole fractions.

As noted in Ref. [2], it must be emphasized that this estimate only accounts for the uncertainty caused by the composition analysis of the samples. All other reasons that could cause the sample to not represent the actual VLE composition are not accounted for in this estimate, but these contributors have been minimized by the measures described in the experimental procedures in Ref. [2] and in Ref. [1].

3.3.6. *Total uncertainty in liquid and vapor phase mole fractions x_{CO_2} and y_{CO_2}*

Like in earlier experiments in Refs. [1, 2], the total uncertainty of the phase equilibrium data were expressed in terms of mole fractions, $u_{tot}(\bar{x}_{CO_2})$ and $u_{tot}(\bar{y}_{CO_2})$, assuming that the combined uncertainty in temperature, pressure and composition measurements are independent of each other. With z equal to x or y for respectively liquid and vapor phase, the total uncertainty was stated as

$$u_{tot}(\bar{z}_{CO_2}) = \sqrt{u_c^2(\bar{z}_{CO_2}) + u_c^2(\bar{T}_f) \cdot \left(\frac{\partial z_{CO_2}}{\partial T}\right)_p^2 + u_c^2(\bar{p}_f) \cdot \left(\frac{\partial z_{CO_2}}{\partial p}\right)_T^2}, \tag{8}$$

where the combined standard uncertainty of the temperature and pressure data points, $u_c(\bar{T}_f)$ and $u_c(\bar{p}_f)$, were calculated as in Section 3.5 in Ref. [1]. The derivatives with respect to temperature and pressure were estimated numerically from the fitted Case 2 EOS, except at higher pressures where the scaling law was used for the derivative with respect to pressure. The fitted EOS and scaling law are described in Section 5.4.2. The combined standard uncertainties of the mole fraction data points were calculated as

$$u_c(\bar{z}_{CO_2}) = \sqrt{s^2(\bar{z}_{CO_2}) + \bar{u}_c^2(z_{CO_2})}, \tag{9}$$

where $s(\bar{z}_{CO_2})$ is the sample standard deviation of the mean of the mole fractions described in Section 3.5 in Ref. [1]. The mean of the systematic standard uncertainty of the mole fractions determined from the composition analysis alone, $\bar{u}_c(z_{CO_2})$, is given in Table 4.

3.4. *Data reduction*

The same procedure for data reduction as used in Ref. [2] was utilized in the present work. For details please refer to Section 3.4 in Ref. [2].

4. Results

VLE measurements at the average temperatures 253.15, 273.16, 283.30 and 298.16 K were conducted, and covered pressures from the vapor pressure of CO_2 up to close to the critical point at each temperature.

The data and corresponding uncertainty terms for each series of samples are given at mean temperature $\bar{T}_f$, mean pressure $\bar{p}_f$ and mean mole fractions for the liquid phase $\bar{x}_{CO_2}$ and the vapor phase $\bar{y}_{CO_2}$ in Tables 5 and 6. These averaged data are plotted with the uncertainties in composition and pressure in Figs. 3a to 3d. The total standard uncertainty of the mole fraction data points, $u_{tot}(\bar{x}_{CO_2})$ and $u_{tot}(\bar{y}_{CO_2})$, which were calculated using the scaling law in Section 5.3, are identified in Tables 5 and 6 using the plus symbol $^+$.

5. Analysis and discussion

5.1. *Summary and analysis of uncertainty estimates*

With reference to Tables 5 and 6, the combined standard uncertainty of the mole fraction data points, $u_c(\bar{z}_{CO_2})$, were dominated by the mean uncertainty stemming from the composition analysis, $\bar{u}_c(z_{CO_2})$ from Table 4. The sample standard deviation of the mean of the mole fractions, $s(\bar{z}_{CO_2})$, did not contribute significantly. This implies that if the composition analysis uncertainty could be lowered, for instance by improving the calibration model in Eq. (6), the combined standard uncertainty could be improved.

The total standard uncertainty in the liquid and vapor phase mole fractions, $u_{tot}(\bar{z}_{CO_2})$, increased as a function of increasing pressure from close to equal to $\bar{u}_c(z_{CO_2})$ from Table 4 up to a maximum value of $8.9 \cdot 10^{-4}$ for bubble point L6 at 253.15 K. At the higher pressures close to the mixture critical points, the uncertainty was influenced more heavily by the pressure uncertainty, as expected by the higher VLE composition sensitivity to pressure in these regions.

5.2. *Comparison with literature data*

The literature data reviews in Refs. [4, 5, 6, 7] provided in total five works reporting isothermal analytic VLE measurements [28, 30, 32, 31, 29]. A summary of these literature data is given in Table 7.

Literature data at temperatures comparable to our measurements are plotted together with our data in Figs. 3a to 3d. The data of Köpke [32] are not included, as these measurements were close to pure CO_2. These figures give a general overview of the varying agreement between our data and the literature data.

The data by Kaminishi et al. [28] agree reasonably well with our data where the two works match in temperature,

This is the accepted version of an article published in Fluid Phase Equilibria
https://doi.org/10.1016/j.fluid.2018.05.006

Table 5
Liquid phase: Experimental VLE data for CO_2 + CO at mean temperature $\bar{T}_f$, mean pressure $\bar{p}_f$, and mean liquid phase mole fraction $\bar{x}_{CO_2}$ [a].

	Data			Temperature			Pressure			Composition				
ID	$\bar{T}_f$ (K)	$\bar{p}_f$ (MPa)	$\bar{x}_{CO_2}$ (-)	$s(\bar{T}_f)$ (K)	$\bar{u}_c(\bar{T})$ (K)	$u_c(\bar{T}_f)$ (K)	$s(\bar{p}_f)$ (MPa)	$\bar{u}_c(\bar{p})$ (MPa)	$u_c(\bar{p}_f)$ (MPa)	$s(\bar{x}_{CO_2})$ (-)	$\bar{u}_c(x_{CO_2})$ (-)	$u_c(\bar{x}_{CO_2})$ (-)	$u_{tot}(\bar{x}_{CO_2})$ (-)	$x_{CO_2,calc}$ (-)
P1	253.152	1.9705[b]	0.99999	4.9e-5	7.3e-3	7.3e-3	6.4e-5	3.5e-4	3.4e-4	-	-	-	-	-
L1	253.152	6.0336	0.90512	7.0e-5	8.5e-3	8.5e-3	8.2e-6	1.1e-3	1.1e-3	2.0e-6	3.2e-4	3.2e-4	3.2e-4	0.91106
L2	253.152	8.0607	0.84956	2.2e-5	8.5e-3	8.5e-3	3.6e-6	1.2e-3	1.2e-3	2.3e-6	3.2e-4	3.2e-4	3.2e-4	0.84880
L3	253.152	9.9904	0.78593	7.2e-5	8.5e-3	8.5e-3	1.0e-5	1.4e-3	1.4e-3	6.6e-6	3.2e-4	3.2e-4	3.3e-4	0.77370
L4	253.152	11.8051	0.70224	4.1e-5	8.2e-3	8.2e-3	1.2e-5	2.7e-3	2.7e-3	1.4e-5	3.2e-4	3.2e-4	3.6e-4[+]	0.67889
L5	253.153	12.4956	0.63715	4.7e-5	8.4e-3	8.4e-3	6.0e-6	2.7e-3	2.7e-3	8.5e-6	3.2e-4	3.2e-4	6.3e-4[+]	0.62445
L6	253.153	12.5447	0.62585	9.3e-5	8.3e-3	8.3e-3	5.5e-6	2.7e-3	2.7e-3	9.9e-6	3.2e-4	3.2e-4	8.9e-4[+]	0.61924
P2	273.160	3.4861[c]	0.99999	8.6e-5	6.2e-3	6.2e-3	3.2e-5	1.1e-3	1.1e-3	-	-	-	-	-
L7	273.159	6.1752	0.93536	1.8e-4	5.9e-3	5.9e-3	5.2e-6	1.1e-3	1.1e-3	1.5e-6	3.2e-4	3.2e-4	3.2e-4	0.93747
L8	273.160	8.1243	0.87986	1.4e-4	5.8e-3	5.8e-3	8.1e-6	1.2e-3	1.2e-3	4.0e-6	3.2e-4	3.2e-4	3.2e-4	0.87747
L9	273.159	8.8718	0.85494	1.1e-4	5.9e-3	5.9e-3	8.2e-6	1.3e-3	1.3e-3	1.3e-5	3.2e-4	3.2e-4	3.3e-4	0.84937
L10	273.160	9.6463	0.82453	1.7e-4	6.0e-3	6.0e-3	8.8e-6	1.4e-3	1.4e-3	8.3e-6	3.2e-4	3.2e-4	3.3e-4	0.81545
L11	273.160	10.5757	0.77169	3.3e-4	5.9e-3	5.9e-3	5.3e-6	2.6e-3	2.6e-3	2.3e-6	3.2e-4	3.2e-4	3.9e-4[+]	0.76161
L12	273.159	10.7579	0.74965	2.8e-5	5.8e-3	5.8e-3	6.3e-6	2.7e-3	2.7e-3	3.6e-6	3.2e-4	3.2e-4	6.1e-4[+]	0.74678
L13	273.159	10.7743	0.74629	1.6e-4	5.9e-3	5.9e-3	5.6e-6	2.7e-3	2.7e-3	4.8e-6	3.2e-4	3.2e-4	7.0e-4[+]	0.74528
P3	283.292	4.5185[d]	0.99999	2.6e-4	1.1e-3	1.1e-3	2.1e-5	1.1e-3	1.1e-3	-	-	-	-	-
L14	283.296	6.0651	0.96208	5.2e-5	9.8e-4	9.8e-4	1.5e-5	1.1e-3	1.1e-3	1.5e-6	3.2e-4	3.2e-4	3.2e-4	0.96337
L15	283.296	8.4148	0.89192	1.2e-4	8.9e-4	9.0e-4	3.9e-5	1.2e-3	1.2e-3	4.5e-6	3.2e-4	3.2e-4	3.2e-4	0.88798
L16	283.295	9.0805	0.86505	5.1e-5	8.6e-4	8.6e-4	7.1e-6	1.3e-3	1.3e-3	8.6e-6	3.2e-4	3.2e-4	3.3e-4	0.85816
L17	283.293	9.5276	0.83998	2.2e-4	1.1e-3	1.2e-3	7.1e-6	1.4e-3	1.4e-3	5.0e-6	3.2e-4	3.2e-4	3.4e-4[+]	0.83255
L18	283.294	9.6772	0.82677	3.3e-4	9.3e-4	9.8e-4	4.2e-6	1.4e-3	1.4e-3	2.0e-6	3.2e-4	3.2e-4	3.6e-4[+]	0.82173
L19	283.295	9.7369	0.81835	1.4e-4	9.6e-4	9.7e-4	2.0e-5	1.4e-3	1.4e-3	7.2e-7	3.2e-4	3.2e-4	4.2e-4[+]	0.81677
P4	298.166	6.4368[e]	0.99999	1.4e-4	1.8e-3	1.8e-3	1.3e-5	1.1e-3	1.1e-3	-	-	-	-	-
L20	298.162	7.0678	0.98234	4.5e-4	1.7e-3	1.7e-3	1.0e-6	1.1e-3	1.1e-3	1.2e-6	3.2e-4	3.2e-4	3.2e-4	0.98209
L21	298.162	7.0713	0.98223	3.3e-4	1.7e-3	1.8e-3	1.0e-5	1.1e-3	1.1e-3	5.1e-7	3.2e-4	3.2e-4	3.2e-4	0.98198
L22	298.164	7.0917	0.98161	2.3e-4	1.8e-3	1.8e-3	6.9e-6	1.1e-3	1.1e-3	5.6e-7	3.2e-4	3.2e-4	3.2e-4	0.98135
L23	298.163	7.4001	0.97200	2.5e-4	1.6e-3	1.6e-3	2.4e-6	1.1e-3	1.1e-3	1.2e-6	3.2e-4	3.2e-4	3.2e-4	0.97117
L24	298.162	7.8502	0.95545	3.5e-4	1.5e-3	1.6e-3	1.1e-5	1.1e-3	1.1e-3	4.2e-6	3.2e-4	3.2e-4	3.2e-4[+]	0.95357
L25	298.163	7.9283	0.95190	1.4e-4	1.6e-3	1.6e-3	6.5e-6	1.1e-3	1.1e-3	4.1e-6	3.2e-4	3.2e-4	3.3e-4[+]	0.94993
L26	298.162	8.0613	0.94376	3.8e-4	1.7e-3	1.7e-3	5.7e-6	1.2e-3	1.2e-3	8.2e-7	3.2e-4	3.2e-4	3.4e-4[+]	0.94284
L27	298.163	8.0936	0.93989	3.2e-4	1.5e-3	1.6e-3	1.3e-5	1.2e-3	1.2e-3	2.2e-6	3.2e-4	3.2e-4	4.3e-4[+]	0.94083

[a] Estimated uncertainty terms:

- $s(\bar{T}_f)$: Sample standard deviation of the mean of the temperatures. See Section 3.5 in Ref. [1].
- $\bar{u}_c(\bar{T})$: Mean of the standard systematic uncertainty of the temperature measurements. See Section 3.5 in Ref. [1].
- $u_c(\bar{T}_f)$: Combined standard uncertainty of the temperature data points. See Eq. (12) in Ref. [1].
- $s(\bar{p}_f)$: Sample standard deviation of the mean of the pressures. See Section 3.5 in Ref. [1].
- $\bar{u}_c(\bar{p})$: Mean of the standard systematic uncertainty of the pressure measurements. See Section 3.5 in Ref. [1].
- $u_c(\bar{p}_f)$: Combined standard uncertainty of the pressure data points. See Eq. (11) in Ref. [1].
- $s(\bar{x}_{CO_2})$: Sample standard deviation of the mean of the mole fractions. See Section 3.5 in Ref. [1].
- $\bar{u}_c(x_{CO_2})$: Mean of the systematic standard uncertainty of the mole fractions from composition analysis alone. See Table 4.
- $u_c(\bar{x}_{CO_2})$: Combined standard uncertainty of the mole fraction data points. Eq. (9): $u_c(\bar{x}_{CO_2}) = \sqrt{s^2(\bar{x}_{CO_2}) + \bar{u}_c^2(x_{CO_2})}$
- $u_{tot}(\bar{x}_{CO_2})$: Total standard uncertainty of the mole fraction data points. Eq. (8): $u_{tot}(\bar{x}_{CO_2}) = \sqrt{u_c^2(\bar{x}_{CO_2}) + u_c^2(\bar{T}_f) \cdot (\partial x_{CO_2}/\partial T)_p^2 + u_c^2(\bar{p}_f) \cdot (\partial x_{CO_2}/\partial p)_T^2}$
- $x_{CO_2,calc}(\bar{T}_f, \bar{p}_f)$: PR-MC-WS-NRTL Case 2 EOS calculated mole fraction.

[+] The derivatives $\partial x_{CO_2}/\partial p$ used in Eq. (8) to obtain $u_{tot}(\bar{x}_{CO_2})$ were calculated using the scaling law in Eq. (10) with the parameters in Table 8 instead of the PR-MC-WS-NRTL Case 2 fitted EOS. See Section 5.3 for details.
[b] Reference CO_2 vapor pressure is 1.9698 ± 0.0006 MPa [27].
[c] Reference CO_2 vapor pressure is 3.4861 ± 0.0010 MPa [27].
[d] Reference CO_2 vapor pressure is 4.5181 ± 0.0013 MPa [27].
[e] Reference CO_2 vapor pressure is 6.4366 ± 0.0019 MPa [27].

This is the accepted version of an article published in Fluid Phase Equilibria
https://doi.org/10.1016/j.fluid.2018.05.006

Table 6
Vapor phase: Experimental VLE data for CO_2 + CO at mean temperature $\bar{T}_f$, mean pressure $\bar{p}_f$, and mean vapor phase mole fraction $\bar{y}_{CO_2}$ [a].

	Data			Temperature			Pressure			Composition				
ID	$\bar{T}_f$ (K)	$\bar{p}_f$ (MPa)	$\bar{y}_{CO_2}$ (-)	$s(\bar{T}_f)$ (K)	$\bar{u}_c(\bar{T})$ (K)	$u_c(\bar{T}_f)$ (K)	$s(\bar{p}_f)$ (MPa)	$\bar{u}_c(\bar{p})$ (MPa)	$u_c(\bar{p}_f)$ (MPa)	$s(\bar{y}_{CO_2})$ (-)	$\bar{u}_c(y_{CO_2})$ (-)	$u_c(\bar{y}_{CO_2})$ (-)	$u_{tot}(\bar{y}_{CO_2})$ (-)	$y_{CO_2,calc}$ (-)
P1	253.152	1.9705[b]	0.99999	4.9e-5	7.3e-3	7.3e-3	6.4e-5	3.5e-4	3.4e-4	-	-	-	-	-
V1	253.152	6.0336	0.47118	1.2e-4	8.5e-3	8.5e-3	2.4e-5	1.1e-3	1.1e-3	8.6e-6	2.6e-4	2.6e-4	2.8e-4	0.48902
V2	253.152	8.0587	0.42746	5.0e-5	8.5e-3	8.5e-3	1.3e-3	1.8e-3	1.3e-3	2.6e-5	2.6e-4	2.6e-4	2.7e-4	0.44985
V3	253.152	9.9905	0.42564	4.5e-5	8.4e-3	8.4e-3	5.0e-6	1.4e-3	1.4e-3	1.1e-5	2.6e-4	2.6e-4	2.7e-4	0.44781
V4	253.152	11.8051	0.46643	5.6e-5	8.2e-3	8.2e-3	3.2e-6	2.7e-3	2.7e-3	6.0e-6	2.6e-4	2.6e-4	3.1e-4[+]	0.47787
V5	253.153	12.4956	0.52545	1.1e-4	8.3e-3	8.3e-3	1.1e-5	2.7e-3	2.7e-3	1.4e-5	2.6e-4	2.6e-4	5.9e-4[+]	0.50906
V6	253.153	12.5447	0.53766	9.3e-5	8.3e-3	8.3e-3	9.9e-6	2.7e-3	2.7e-3	9.8e-6	2.6e-4	2.6e-4	8.6e-4[+]	0.51264
P2	273.160	3.4861[c]	0.99999	8.6e-5	6.2e-3	6.2e-3	3.2e-5	1.1e-3	1.1e-3	-	-	-	-	-
V7	273.160	6.1752	0.70553	1.4e-4	5.9e-3	5.9e-3	4.7e-6	1.1e-3	1.1e-3	1.6e-5	2.6e-4	2.6e-4	2.8e-4	0.71636
V8	273.160	8.1233	0.63519	9.6e-5	6.0e-3	6.0e-3	9.4e-4	2.0e-3	1.7e-3	6.5e-6	2.6e-4	2.6e-4	2.7e-4	0.65049
V9	273.159	8.8718	0.62543	1.3e-4	6.0e-3	6.0e-3	1.8e-5	1.3e-3	1.3e-3	3.5e-6	2.6e-4	2.6e-4	2.7e-4	0.64067
V10	273.160	9.6463	0.62597	7.9e-5	5.8e-3	5.8e-3	6.3e-6	1.4e-3	1.4e-3	5.0e-6	2.6e-4	2.6e-4	2.7e-4	0.63904
V11	273.158	10.5757	0.65411	2.7e-4	6.0e-3	6.0e-3	7.0e-6	2.6e-3	2.6e-3	8.6e-6	2.6e-4	2.6e-4	3.4e-4[+]	0.65385
V12	273.159	10.7579	0.67490	6.9e-5	5.7e-3	5.7e-3	1.7e-5	2.7e-3	2.7e-3	6.6e-5	2.6e-4	2.7e-4	5.8e-4[+]	0.66143
V13	273.159	10.7743	0.67839	2.2e-4	5.8e-3	5.8e-3	1.4e-5	2.7e-3	2.7e-3	6.9e-5	2.6e-4	2.7e-4	6.7e-4[+]	0.66228
P3	283.292	4.5185[d]	0.99999	2.6e-4	1.1e-3	1.1e-3	2.1e-5	1.1e-3	1.1e-3	-	-	-	-	-
V14	283.295	6.0651	0.84456	2.8e-4	9.8e-4	1.0e-3	1.5e-5	1.1e-3	1.1e-3	1.3e-5	2.6e-4	2.6e-4	2.7e-4	0.85087
V15	283.296	8.3988	0.74612	1.5e-4	9.3e-4	9.4e-4	1.1e-5	1.2e-3	1.2e-3	7.5e-6	2.6e-4	2.6e-4	2.6e-4	0.75704
V16	283.295	9.0805	0.74186	4.2e-4	9.1e-4	1.0e-3	8.1e-6	1.3e-3	1.3e-3	3.2e-6	2.6e-4	2.6e-4	2.6e-4	0.75062
V17	283.293	9.5276	0.75116	1.1e-4	1.3e-3	1.3e-3	1.1e-5	1.4e-3	1.4e-3	2.9e-6	2.6e-4	2.6e-4	2.7e-4[+]	0.75385
V18	283.294	9.6769	0.76098	6.8e-4	1.0e-3	1.2e-3	2.4e-4	1.4e-3	1.4e-3	2.5e-5	2.6e-4	2.6e-4	2.9e-4[+]	0.75747
V19	283.294	9.7366	0.76886	9.5e-5	1.1e-3	1.1e-3	2.1e-4	1.4e-3	1.4e-3	2.7e-5	2.6e-4	2.6e-4	3.6e-4[+]	0.75958
P4	298.166	6.4368[e]	0.99999	1.4e-4	1.8e-3	1.8e-3	1.3e-5	1.1e-3	1.1e-3	-	-	-	-	-
V20	298.163	7.0678	0.95929	9.5e-5	1.6e-3	1.6e-3	1.5e-5	1.1e-3	1.1e-3	1.0e-6	2.6e-4	2.6e-4	2.7e-4	0.96187
V21	298.164	7.0918	0.95791	7.8e-5	1.7e-3	1.7e-3	1.2e-5	1.1e-3	1.1e-3	1.7e-5	2.6e-4	2.6e-4	2.7e-4	0.96065
V22	298.162	7.4001	0.94291	2.0e-4	1.5e-3	1.5e-3	9.0e-6	1.1e-3	1.1e-3	1.2e-6	2.6e-4	2.6e-4	2.6e-4	0.94619
V23	298.162	7.8502	0.92781	2.2e-4	1.5e-3	1.6e-3	1.4e-5	1.1e-3	1.1e-3	3.9e-6	2.6e-4	2.6e-4	2.6e-4[+]	0.93060
V24	298.163	7.9283	0.92663	9.6e-5	1.5e-3	1.5e-3	6.5e-6	1.1e-3	1.1e-3	7.1e-6	2.6e-4	2.6e-4	2.6e-4[+]	0.92880
V25	298.163	8.0232	0.92650	7.1e-5	1.5e-3	1.5e-3	9.9e-6	1.2e-3	1.2e-3	4.4e-6	2.6e-4	2.6e-4	2.6e-4[+]	0.92718
V26	298.162	8.0613	0.92747	1.0e-4	1.5e-3	1.5e-3	8.5e-6	1.2e-3	1.2e-3	2.6e-6	2.6e-4	2.6e-4	2.6e-4[+]	0.92677
V27	298.163	8.0936	0.93007	1.9e-4	1.5e-3	1.5e-3	6.4e-6	1.2e-3	1.2e-3	2.9e-6	2.6e-4	2.6e-4	3.4e-4[+]	0.92661

[a] Estimated uncertainty terms are described in Table 5, but with x instead of y.
[+] The derivatives $\partial y_{CO_2}/\partial p$ used in Eq. (8) to obtain $u_{tot}(\bar{y}_{CO_2})$ were calculated using the scaling law in Eq. (10) with the parameters in Table 8 instead of the PR-MC-WS-NRTL Case 2 fitted EOS. See Section 5.3 for details.
[b] Reference CO_2 vapor pressure is 1.9698 ± 0.0006 MPa [27].
[c] Reference CO_2 vapor pressure is 3.4861 ± 0.0010 MPa [27].
[d] Reference CO_2 vapor pressure is 4.5181 ± 0.0013 MPa [27].
[e] Reference CO_2 vapor pressure is 6.4366 ± 0.0019 MPa [27].

Table 7
Available isothermal (ISOT), synthetic/constant-composition (ISOC) VLE and critical point (CP) literature data and the temperature, pressure and composition ranges.

Authors	Year	Type	T (K)	p (MPa)	Composition CO_2	No. of points
Kaminishi et al. [28]	1968	ISOT	223, 233, 253, 273, 283	2.39-13.08	0.213-0.957	40
Christiansen et al. [30]	1974	ISOT	223, 243, 263, 283	0.68-14.15	0.2-0.9972	68
Ke et al. [31]	2001	CP	280.2, 283.5, 289.0, 292.5, 298.2	9.92-8.10	0.729, 0.773, 0.841, 0.878, 0.930	5
Köpke [32]	2010	ISOC	243.5-292.7	1.44-5.63	0.998418-0.999932	32
Blanco et al. [29]	2014	ISOC	253.15, 263.15, 273.15, 283.15, 293.15	1.97-7.47	0.9700, 0.9810, 0.9902, 0.9930, 0.9960	50

This is the accepted version of an article published in Fluid Phase Equilibria
https://doi.org/10.1016/j.fluid.2018.05.006

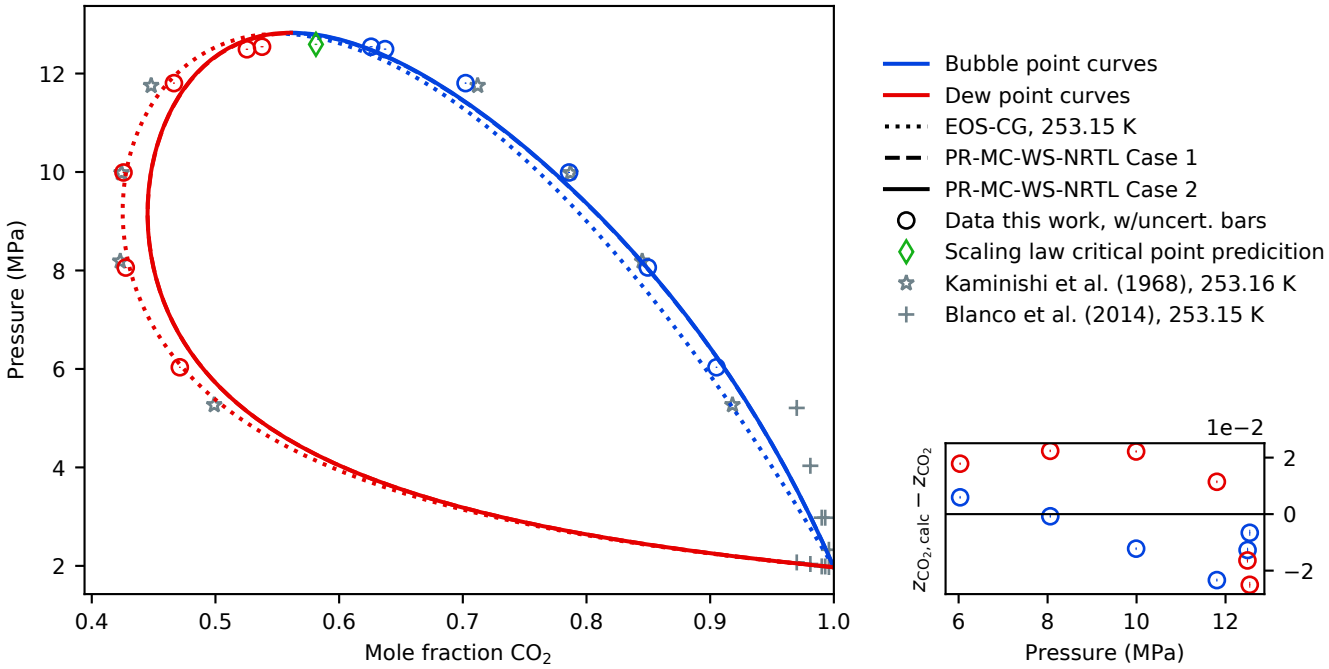

(a) Mean temperature of measurements and models in present work 253.153 K. VLE data from literature Kaminishi et al. [28], Blanco et al. [29].

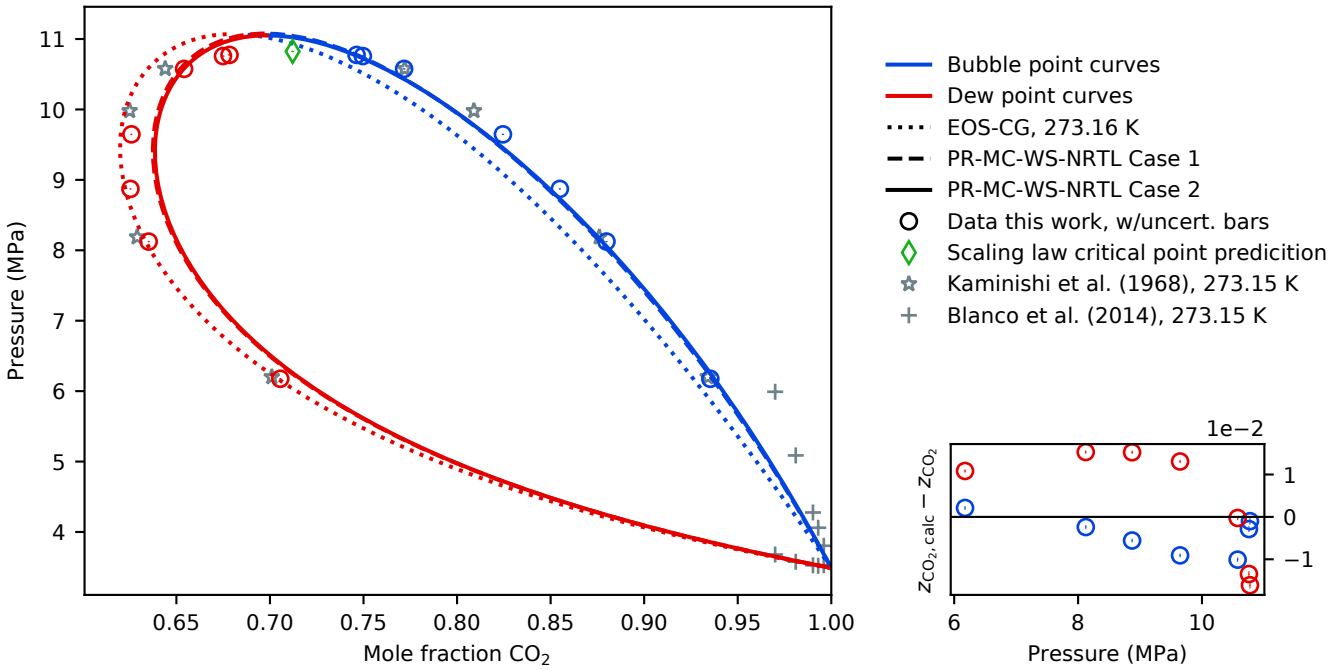

(b) Mean temperature of measurements and models in present work 273.159 K. VLE data from literature Kaminishi et al. [28], Blanco et al. [29].

This is the accepted version of an article published in Fluid Phase Equilibria
https://doi.org/10.1016/j.fluid.2018.05.006

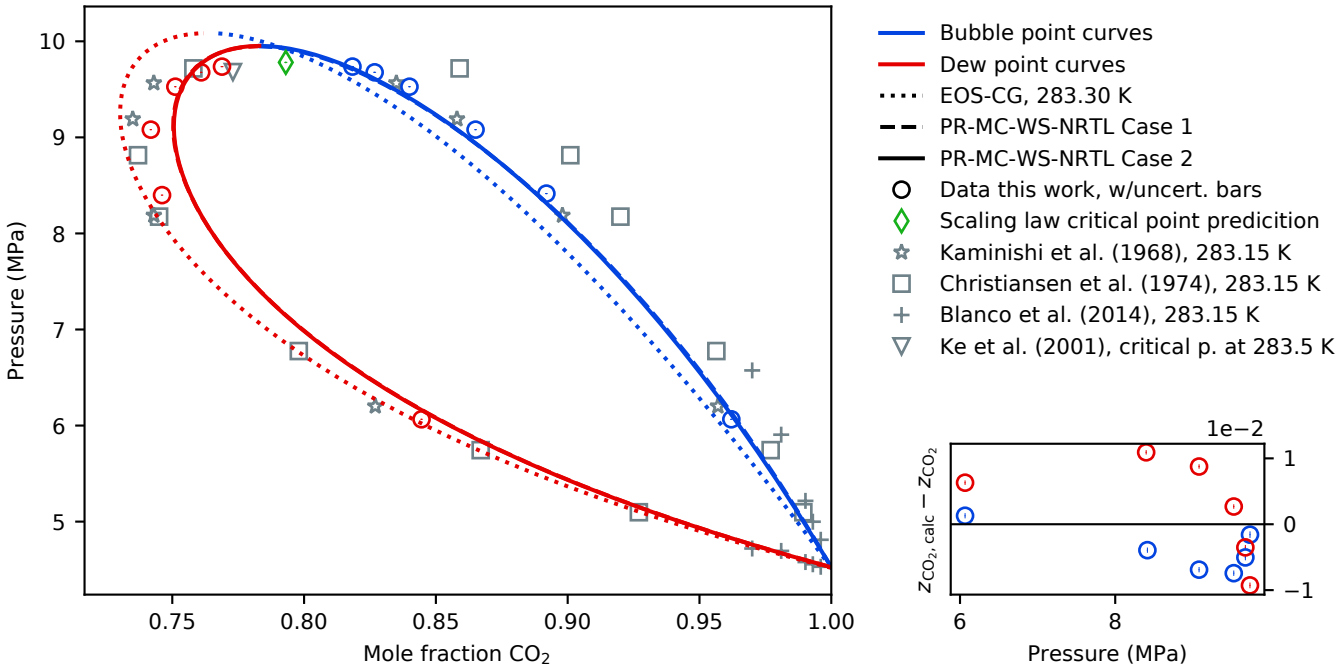

(c) Mean temperature of measurements and models in present work 283.295 K. VLE data from literature Kaminishi et al. [28], Christiansen et al. [30], Blanco et al. [29], Ke et al. [31].

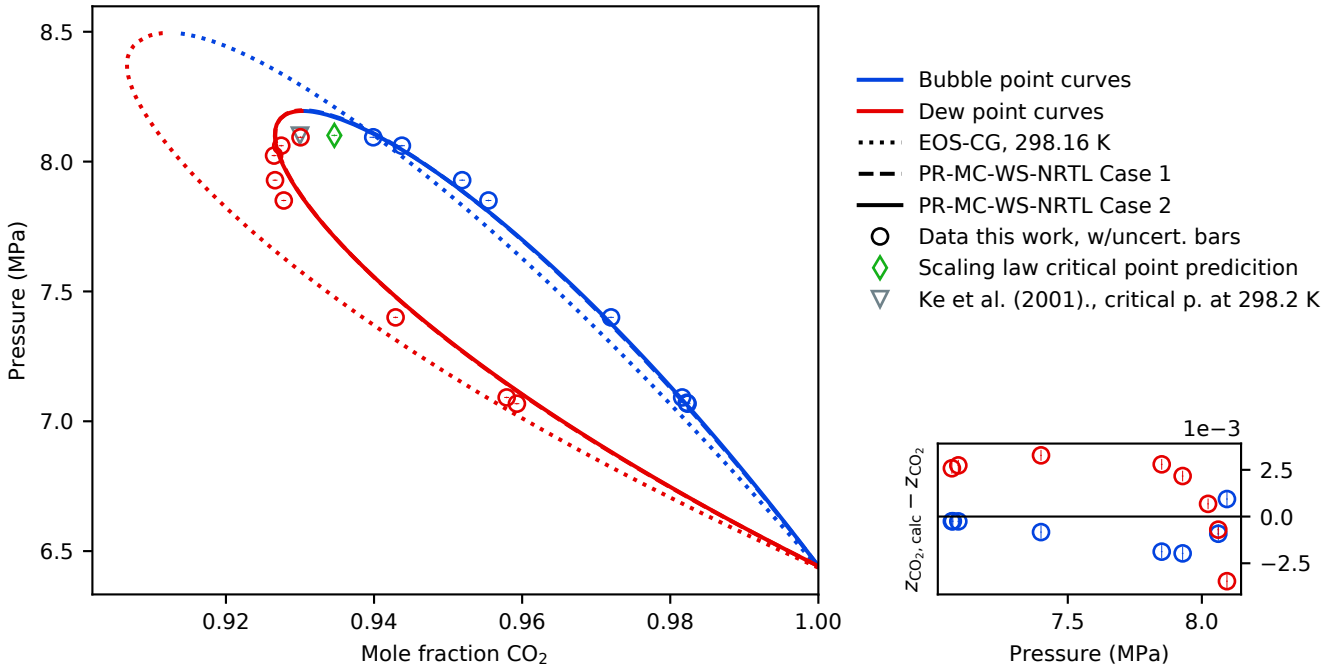

(d) Mean temperature of measurements and models in present work 298.163 K. VLE data from literature Ke et al. [31].

Fig. 3. Four VLE isotherms measured in this work: Left of all subfigures: Pressure-composition diagram based on EOS calculations at the different mean temperatures, VLE data from literature, and VLE measurements with estimated uncertainties from present work: $\bar{x}_{CO_2}$, $\bar{y}_{CO_2}$, $\bar{p}_f$, $u_{tot}(\bar{x}_{CO_2})$, $u_{tot}(\bar{y}_{CO_2})$ and $u_c(\bar{p}_f)$ from Tables 5 and 6. Please note that the uncertainty bars are very small compared to the scale of the plots. Critical point estimation and its uncertainties are from Section 5.3. Right of all subfigures: Plot of deviation between PR-MC-WS-NRTL Case 2 $z_{CO_2,calc}$ and VLE measurements from present work z_{CO_2}, where z_{CO_2} is equal to either x_{CO_2} or y_{CO_2}. Please see online version of article for plot details.

This is the accepted version of an article published in Fluid Phase Equilibria
https://doi.org/10.1016/j.fluid.2018.05.006

although with larger deviations in the vapor phase than the liquid phase. The vapor phase data by Christiansen et al. [30] at 283 K agree well with our data in the vapor phase at low pressures, but the deviations are quite large for the liquid phase data at the highest pressures, in the order of 3-4 mole-%. The vapor phase data by Blanco et al. [29] are difficult to compare with our data, but their liquid phase data seem to deviate significantly from our data and those by Kaminishi et al. [28]. The critical point data by Ke et al. [31] agree well with our scaling law estimates in terms of pressure, but are between 0.5 to 2 mole-% lower in CO_2 mole fractions.

As can be seen from Figs. 3a to 3d, the agreement between our data and literature data varies significantly, especially in the liquid phase measurements. The data in the present work describes the VLE at four different temperatures, and show considerably less scatter than the available literature data. In addition, at each temperature, the present work provide data closer to the mixture critical points than previously available, thus providing a good foundation for model fitting and validation. Finally, the present work provide the only complete VLE isotherm at temperatures above 283 K.

5.3. Critical point estimation

To estimate the mixture critical points at each isotherm, a scaling law was utilized [33, 34]:

$$z_{CO_2} = \hat{z}_{CO_2,c} + \left(\lambda_1 - \epsilon\frac{\lambda_2}{2}\right)(\hat{p}_c - p) - \epsilon\frac{\mu}{2}(\hat{p}_c - p)^{\beta} \quad , \quad \text{where} \quad \epsilon = \begin{cases} 1 \text{ for bubble points,} \\ -1 \text{ for dew points,} \end{cases} \tag{10}$$

and z_{CO_2} was the bubble point ($z_{CO_2} = x_{CO_2}$) or dew point ($z_{CO_2} = y_{CO_2}$) CO_2 mole fraction at pressure p. Utilizing the VLE data in the critical region identified in Table 8, the critical composition $z_{CO_2,c}$ and pressure p_c of the scaling law were fitted using ordinary unweighted least squares. The value of β was fixed at 0.325 [35]. The estimators $\hat{z}_{CO_2,c}$, $\hat{p}_c$, $\hat{\mu}$, $\hat{\lambda}_1$ and $\hat{\lambda}_2$ are given in Table 8.

Employing Eqs. (16) and (17) in Ref. [1], the estimated uncertainties in the critical composition and pressure estimates were calculated as $u(\hat{z}_{CO_2,c})$ and $u(\hat{p}_c)$.

The uncertainty estimates in the composition of the VLE data utilized in the scaling law fitting, $u_{tot}(\bar{x}_{CO_2})$ and $u_{tot}(\bar{y}_{CO_2})$, were calculated in the same manner as in Ref. [2], and indicated with the plus symbol $^+$ in Tables 5 and 6.

The estimated critical compositions and pressures with their corresponding uncertainties are given in Table 8, and are plotted together with the critical region VLE data in Fig. 4.

5.4. Model fitting

5.4.1. Introduction

As noted in Section 1, the modeling of the thermodynamics of the CO_2+CO system has been restricted by the the lack of high quality data and inconsistencies in existing data, for example in the development of the EOS-CG equation of state [5, 6]. There are hence room for model improvements on this binary system.

Calculations with the EOS-CG model were performed using our in-house thermodynamics library described in Wilhelmsen et al. [36]. The calculated pressure-composition VLE behavior are shown in Figs. 3a to 3d. As can be seen from these Figures, the deviations between the EOS-CG model and the VLE data in the present work are most pronounced at higher temperatures, where no data could be found in literature from before. The VLE data provided in the present work, together with other thermodynamic data such as speed of sound and density, allow for an enhanced fit of EOS-CG.

In this work, the parameters of the Peng-Robinson (PR) cubic EOS [37] with the alpha correction by Mathias and Copeman [38] (MC), the mixing rules by Wong and Sandler [39] (WS), and the NRTL [40] excess Gibbs energy model were fitted to the new data. This combination was designated as PR-MC-WS-NRTL for the present work, and details regarding the formulas can be found in Ref. [1]. Some success in utilizing this combination for fitting binary system VLE data with one supercritical component has been obtained in our previous works Ref. [2] (CO_2+O_2), Ref. [1] (CO_2+N_2), Ref. [14] (CO_2+CH_4), Ref.[15] and in the work of Coquelet et al. [41] (CO_2+Ar).

The model fit was performed using orthogonal distance regression (ODR) [42], utilizing the VLE data in Tables 5 and 6. For details regarding our use of ODR, please refer to Section 5.4 in Ref. [2].

5.4.2. Fit of Peng-Robinson EOS

The adjustable parameters of the PR-MC-WS-NRTL EOS consist of the binary interaction parameters of the NRTL model, τ_{ij}, the non-randomness parameters of the NRTL model, α_{ij}, and the Wong-Sandler binary interaction parameters, k_{ij}. These parameters were restricted according to Eq. (27) in Ref. [1], and for a system of two non-polar components such as CO_2+COa constant value for $\alpha_{12} = \alpha_{21} = 0.3$ was assumed [40] (cf. Refs. [2, 41]). The component-specific EOS parameters critical temperature, critical pressure and MC alpha correction parameters, are given in Table 10.

The remaining three adjustable parameters, k_{12}, τ_{12} and τ_{21}, were assumed to be temperature dependent. First, these parameters were fitted against the data in the present work at each of the four average temperatures (Case 1) using our in-house thermodynamics library [36]. The resulting parameters are given in Table 9. Second, the Case 1 parameters formed the basis for finding a model which could represent the parameter temperature behavior, thus enabling the use of the EOS over the whole temperature range of the VLE data (Case 2).

The temperature dependencies of τ_{12} and τ_{21} could be approximately described by the following functions:

$$\tau_{12}(T) = a_{\tau_{12}} + b_{\tau_{12}} \cdot T + c_{\tau_{12}} \cdot T^2 \, , \tag{11}$$

$$\tau_{21}(T) = a_{\tau_{21}} + b_{\tau_{21}} \cdot T + c_{\tau_{21}} \cdot T^2 \, . \tag{12}$$

This is the accepted version of an article published in Fluid Phase Equilibria
https://doi.org/10.1016/j.fluid.2018.05.006

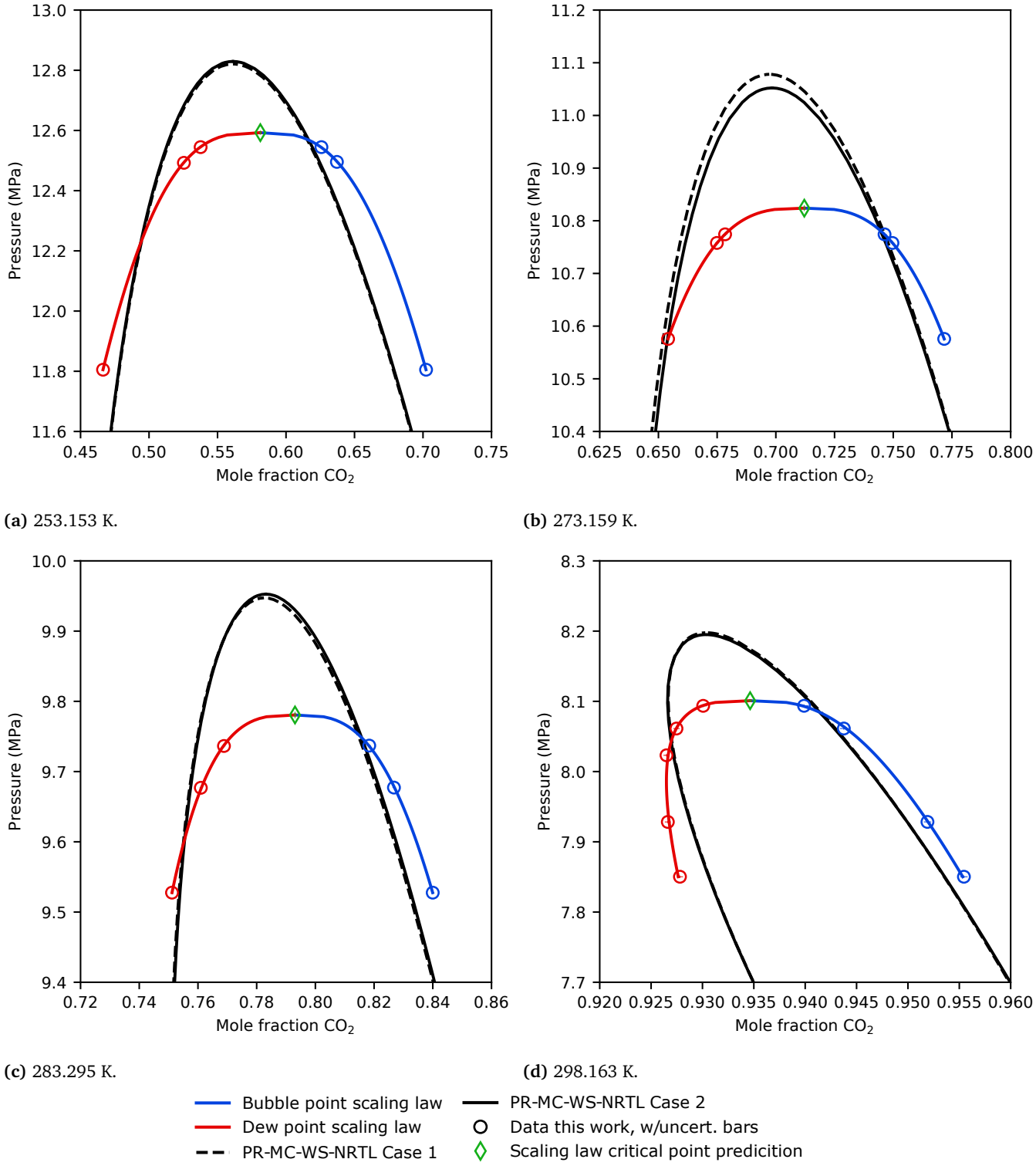

(a) 253.153 K.

(b) 273.159 K.

(c) 283.295 K.

(d) 298.163 K.

Fig. 4. Comparison of the predictions of the pressure-composition phase behavior in the critical region by three different models: PR-MC-WS-NRTL Case 1 and Case 2 EOSs, and the scaling law model in Eq. (10). Please note that the scales of the graphs are different from each other. Please refer to Table 8 for an overview of the VLE points used to fit the scaling law and the parameters at the different temperatures.

This is the accepted version of an article published in Fluid Phase Equilibria
https://doi.org/10.1016/j.fluid.2018.05.006

Table 8
Parameters of the scaling law in Eq. (10) fitted to critical region data[a] from this work at four different average temperatures, with uncertainty estimates[b].

T (K)	Used points[a]	n_p (-)	$\hat{\lambda}_1$ (MPa^{-1})	$\hat{\lambda}_2$ (MPa^{-1})	$\hat{\mu}$ (MPa$^{-\beta}$)	$\hat{z}_{CO_2,c}$ (-)	$\hat{p}_c$ (MPa)	$S_E(\hat{z}_{CO_2,c})$ (-)	$u(\hat{z}_{CO_2,c})$ (-)	$S_E(\hat{p}_c)$ (MPa)	$u(\hat{p}_c)$ (MPa)
253.153	L4-6, V4-6	6	$3.8490 \cdot 10^{-3}$	$-2.5888 \cdot 10^{-2}$	−0.232 78	0.5812	12.593	$3.7 \cdot 10^{-4}$	$7.1 \cdot 10^{-4}$	$4.8 \cdot 10^{-3}$	$5.5 \cdot 10^{-3}$
273.159	L11-13, V11-13	6	$3.1280 \cdot 10^{-3}$	$-1.8742 \cdot 10^{-2}$	−0.177 64	0.7121	10.824	$1.0 \cdot 10^{-4}$	$5.6 \cdot 10^{-4}$	$3.9 \cdot 10^{-3}$	$4.7 \cdot 10^{-3}$
283.295	L17-19, V17-19	6	$9.8720 \cdot 10^{-3}$	$-7.4910 \cdot 10^{-3}$	−0.135 84	0.7931	9.781	$2.1 \cdot 10^{-4}$	$4.0 \cdot 10^{-4}$	$3.8 \cdot 10^{-3}$	$4.0 \cdot 10^{-3}$
298.163	L24-27, V23-27	9	$2.7318 \cdot 10^{-2}$	$1.3643 \cdot 10^{-2}$	−0.048 77	0.9346	8.101	$1.2 \cdot 10^{-4}$	$3.3 \cdot 10^{-4}$	$1.0 \cdot 10^{-3}$	$1.6 \cdot 10^{-3}$

[a] Pressure-Composition data and uncertainties from Tables 5 and 6, identified with the given IDs.
[b] Estimated uncertainty terms:

- Standard uncertainties in the estimated critical composition: $u(\hat{z}_{CO_2,c}) = \sqrt{S_E^2(\hat{z}_{CO_2,c}) + (\sum^{n_p} u_{tot}(\bar{z}_{CO_2})/n_p)^2}$, from Eq. (16) in [1].
- Standard uncertainties in the estimated critical pressure: $u(\hat{p}_c) = \sqrt{S_E^2(\hat{p}_c) + (\sum^{n_p} u_c(\bar{p}_f)/n_p)^2}$, from Eq. (17) in [1].
- Standard errors of regression of the critical composition and pressure, $S_E(\hat{z}_{CO_2,c})$ and $S_E(\hat{p}_c)$. See [1] for details.

Table 9
Optimal parameters k_{12}, τ_{12} and τ_{21} for the PR-MC-WS-NRTL model, fitted against data from the present work Absolute average deviation AAD[c] and bias BIAS[d].

	Case 1[a]				
T (K)	k_{12}	τ_{12}	τ_{21}		
253.153	0.103546	2.183291	-0.985210		
273.159	0.117090	2.292420	-1.096713		
283.295	0.130598	2.700040	-1.263041		
298.163	0.109134	2.281289	-1.043499		
	Case 2[b]				
T (K)	k_{12}	τ_{12}	τ_{21}	AAD (%)	BIAS (%)
253.153	0.12	2.500493	-1.071152	1.47	0.14
273.159	0.12	2.375723	-1.125613	0.84	0.03
283.295	0.12	2.470851	-1.180281	0.56	0.06
298.163	0.12	2.803062	-1.293417	0.16	-0.03

[a] $k_{12} = k_{21}$, τ_{12}, τ_{21}: varies freely, $\alpha = 0.3$
[b] $k_{12} = k_{21} = 0.12$, $\alpha = 0.3$. τ_{12}, and τ_{21} calculated from Eqs. (11) and (12) respectively using $a_{\tau_{12}} = 39.91838$, $b_{\tau_{12}} = -2.790\,096 \cdot 10^{-1}$, $c_{\tau_{12}} = 5.182\,724 \cdot 10^{-4}$, $a_{\tau_{21}} = -6.510336$, $b_{\tau_{21}} = 4.392\,077 \cdot 10^{-2}$ and $c_{\tau_{21}} = -8.862\,232 \cdot 10^{-5}$.
[c] AAD $= (100/n)\sum|z_{i,CO_2} - z_{i,CO_2,calc}|$
[d] BIAS $= (100/n)\sum(z_{i,CO_2} - z_{i,CO_2,calc})$

The fitted parameters of Eqs. (11) and (12) and the calculated values of τ_{12}, τ_{21}, and k_{12} are given in Table 9, denoted as Case 2.

The VLE predictions of the PR-MC-WS-NRTL model using both the Case 1 and 2 parameters are shown in Figs. 3a to 3d together with the data from this work and literature. In addition, the deviations between the Case 2 calculated mole fractions and the experimental values are plotted in these figures. The absolute average deviation and bias for Case 2 are given in Table 9. As the Figures show, the difference between the Case 1 and 2 parameters are very small, and therefore only the Case 2 representation will be discussed in what follows.

Two aspects of the Case 2 model could be observed with respect to the measurement data from the present work. The critical point estimates from the scaling law in Section 5.3 match those of the Case 2 model quite well. The critical pressures estimated by the Case 2 model are approximately 2% higher than the pressures predicted by the scaling law, and the differences in critical compositions are less than 0.02. As the pressure-composition deviation plots indicate at each isotherm, the composition deviations seem to develop in a similar manner as function of pressure, without apparent scatter present. As argued in Ref. [2], the presence of scatter would lead to suspicion that the deviant compositions were in fact not representative the actual VLE state. To be precise, the absence of scatter indicates that the samples were representative of the actual VLE composition, however not necessarily that the measured mole fractions for these samples were correct.

Considering the previous discussion, the PR-MC-WS-NRTL Case 2 model provides a seemingly accurate description of the VLE for the CO_2+CO system given by the data from the present work from the temperatures 253 to 298 K, with an AAD of maximum 0.015 in mole fraction and an apparently good description of the critical locus.

Table 10
Critical properties[a] and Mathias-Copeman coefficients[b] used in PR-MC-WS-NRTL EOS for CO_2 and CO.

i	$T_{c,i}$ (K)	$p_{c,i}$ (MPa)	$c_{1,i}$	$c_{2,i}$	$c_{3,i}$
CO_2	304.2	7.3765	0.704606	-0.314862	1.89083
CO	132.85	3.494	0.7050	-0.3185	1.9012

[a] CO_2: From in-house thermodynamics library described in Wilhelmsen et al. [36]. CO: From Chiavone-Filho et al. [43]. Slightly different from the values used in reference EOSs [27] and [44, 45]: $T_{c,CO_2} = 304.1282$ K, $p_{c,CO_2} = 7.3773$ MPa, $T_{c,CO} = 132.86$ K, $p_{c,CO} = 3.494$ MPa.
[b] CO_2: From in-house thermodynamics library described in Wilhelmsen et al. [36], which is slightly different than values in [43]. CO: From Chiavone-Filho et al. [43].

6. Conclusions

The current work reports vapor-liquid equilibrium (VLE) data for the CO_2+CO binary system, at the temperatures 253.15, 273.16, 283.30 and 298.16 K with very high accuracy.

At these isotherms the composition spans a large range of VLE liquid and vapor phase compositions, from approximately 0.63 to 0.982 CO_2 mole fractions in the liquid phase and from 0.43 to 0.959 in the vapor phase. The CO_2 vapor pressure is measured at each temperature and compared with values calculated with the Span-Wagner EOS for CO_2. The measured CO_2 vapor pressure is consistent with the calculated values when the expanded uncertainty is counted for both in the measurements and the calculated values from the

This is the accepted version of an article published in Fluid Phase Equilibria
https://doi.org/10.1016/j.fluid.2018.05.006

EOS. The measurements presented in this study shows significant deviations compared with literature data, especially in the liquid phase measurements. It has earlier been reported inconsistencies in the literature data in [4, 5, 6, 7]. Several stable measurements close to the mixture critical point at each isotherm combined with a scaling law [33, 34], results in precise estimates for the mixture critical points.

The data presented in this work show little scatter compared to the data found in the literature. Also the multiple measurements in the proximity of the mixture critical points for all the isotherms support the quality of the measurements. A detailed analysis of the uncertainties of the measurements are provided.

Each of the four isotherms in the present work was fitted to the Peng-Robinson (PR) cubic EOS [37] with the alpha correction by Mathias and Copeman [38] (MC), the mixing rules by Wong and Sandler [39] (WS), and the NRTL [40] excess Gibbs energy model. The fitted model parameters at each isotherms were also fitted to a second order polynomial in temperature. The resulting EOS can be utilized for VLE calculations over the temperature range from 253 to 298 K. This EOS represents the data with a good accuracy. The absolute average deviation between the measured datapoints and the model calculated and compared for each temperature, and the maximum deviation is 0.015 in mole fraction. The model also resemble the critical points given by the scaling law predictions. The deviation in calculated critical pressure by the PR-MC-WS-NRTL model are approximately 2% above the scaling law. The corresponding difference in mole fraction is less 0.02 when compared to the results from the scaling law.

This work contributes significantly to improve the available data point for the CO_2+CO system. The added data can be used to improve very flexible multi-parameter equations of state such as EOS-CG [5, 6]. EOS-CG should be able to describe all the thermodynamic properties of the system better than the fitted equations in the PR-MC-WS-NRTL model fit presented in this work.

Acknowledgements

The research leading to these results has received funding from the Norwegian Financial Mechanism 2009-2014 under Project Contract no. 7F14466.

This publication has been produced with support from the NCCS Centre, performed under the Norwegian research program Centres for Environment-friendly Energy Research (FME). The authors acknowledge the following partners for their contributions: Aker Solutions, ANSALDO Energia, CoorsTek Membrane Sciences, Gassco, KROHNE, Larvik Shipping, Norcem, Norwegian Oil and Gas, Quad Geometrics, Shell, Statoil, TOTAL, and the Research Council of Norway (257579/E20)

The authors would like to thank Håvard Rekstad and Reidar Tellebon of NTNU. We would also like to thank SINTEF Energy Research interns Ranisha Sitlapersad and Caroline Einen for their contributions.

Finally, the authors would like to thank Professor Roland Span of Ruhr-Universität Bochum and Dr. Johannes Gernert for the access to their literature data base [5].

References

[1] S. F. Westman, H. G. J. Stang, S. W. Løvseth, A. Austegard, I. Snustad, S. Ø. Størset, I. S. Ertesvåg, Vapor-liquid equilibrium data for the carbon dioxide and nitrogen (CO_2 + N_2) system at the temperatures 223, 270, 298 and 303 K and pressures up to 18 MPa, Fluid Phase Equilib. 409 (2016) 207–241, URL http://dx.doi.org/10.1016/j.fluid.2015.09.034.

[2] S. F. Westman, H. G. J. Stang, S. W. Løvseth, A. Austegard, I. Snustad, I. S. Ertesvåg, Vapor-liquid equilibrium data for the carbon dioxide and oxygen (CO_2 + O_2) system at the temperatures 218, 233, 253, 273, 288 and 298 K and pressures up to 14 MPa, Fluid Phase Equilib. 421 (2016) 67–87, URL http://dx.doi.org/10.1016/j.fluid.2016.04.002.

[3] Energy Technology Perspectives 2016 – Towards Sustainable Urban Energy Systems, Tech. Rep., International Energy Agency, Paris, France, URL http://www.iea.org/etp/, 2016.

[4] S. T. Munkejord, M. Hammer, S. W. Løvseth, CO_2 transport: Data and models – a review, Appl. Energy 169 (2016) 499–523, URL http://dx.doi.org/10.1016/j.apenergy.2016.01.100.

[5] J. Gernert, R. Span, EOS-CG: A Helmholtz energy mixture model for humid gases and CCS mixtures, J. Chem. Thermodyn. 93 (2016) 274–293, URL http://dx.doi.org/10.1016/j.jct.2015.05.015.

[6] G. J. Gernert, A New Helmholtz Energy Model for Humid Gases and CCS Mixtures, PhD dissertation, Fakultät für Maschinenbau, Ruhr-Universität Bochum, Bochum, URL http://www-brs.ub.ruhr-uni-bochum.de/netahtml/HSS/Diss/GernertGeorgJohannes/diss.pdf, 2013.

[7] H. Li, J. P. Jakobsen, Ø. Wilhelmsen, J. Yan, PVTxy Properties of CO_2 Mixtures Relevant for CO_2 Capture, Transport and Storage: Review of Available Experimental Data and Theoretical Models, Appl. Energy 88 (11) (2011) 3567–3579, URL http://dx.doi.org/10.1016/j.apenergy.2011.03.052.

[8] S. W. Løvseth, G. Skaugen, H. G. J. Stang, J. P. Jakobsen, Ø. Wilhelmsen, R. Span, R. Wegge, CO_2Mix Project: Experimental Determination of Thermo-Physical Properties of CO_2-Rich Mixtures, Energy Procedia 37 (2013) 2888–2896, URL http://dx.doi.org/10.1016/j.egypro.2013.06.174.

[9] G. Skaugen, S. Roussanaly, J. Jakobsen, A. Brunsvold, Techno-economic evaluation of the effects of impurities on conditioning and transport of CO2 by pipeline, Int. J. Greenhouse Gas Control 54 (Part 2) (2016) 627 – 639, URL http://dx.doi.org/10.1016/j.ijggc.2016.07.025.

[10] R. T. Porter, M. Fairweather, M. Pourkashanian, R. M. Woolley, The range and level of impurities in CO_2 streams from different carbon capture sources, Int. J. Greenhouse Gas Control 36 (2015) 161–174, URL http://dx.doi.org/10.1016/j.ijggc.2015.02.016.

[11] H. G. J. Stang, S. W. Løvseth, S. Ø. Størset, B. Malvik, H. Rekstad, Accurate Measurements of CO_2 Rich Mixture Phase Equilibria Relevant for CCS Transport and Conditioning, Energy Procedia 37 (2013) 2897–2903, URL http://dx.doi.org/10.1016/j.egypro.2013.06.175.

[12] E. De Visser, C. Hendriks, M. Barrio, M. J. Mølnvik, G. de Koeijer, S. Liljemark, Y. Le Gallo, Dynamis CO_2 Quality Recommendations, Int. J. Greenhouse Gas Control 2 (4) (2008) 478–484, URL http://dx.doi.org/10.1016/j.ijggc.2008.04.006.

[13] S. W. Løvseth, H. G. J. Stang, A. Austegard, S. F. Westman, R. Span, R. Wegge, Measurements of CO_2-Rich Mixture Properties: Status and CCS Needs, Energy Procedia 86 (2016) 469–478, URL http://dx.doi.org/10.1016/j.egypro.2016.01.048, the 8th Trondheim Conference on CO2 Capture, Transport and Storage.

[14] E. Petropoulou, E. Voutsas, S. F. Westman, A. Austegard, H. G. J. Stang, S. W. Løvseth, Vapor - liquid equilibrium of the carbon dioxide/methane mixture at three isotherms, submitted to a peer-reviewed journal.

[15] S. W. Løvseth, A. Austegard, S. F. Westman, H. G. J. Stang, S. Herrig, T. Neumann, R. Span, Thermodynamics of the carbon dioxide plus argon (CO_2 + Ar) system: An improved reference mixture model and measurements of vapor-liquid, vapor-solid, liquid-solid and vapor-liquid-solid phase equilibrium data at the temperatures 213 to 299 K and pressures up to 16 MPa, submitted to a peer-reviewed journal.

[16] R. D. Chirico, T. W. de Loos, J. Gmehling, A. R. H. Goodwin, S. Gupta, W. M. Haynes, K. N. Marsh, V. Rives, J. D. Olson, C. Spencer, J. F. Brennecke, J. P. M. Trusler, Guidelines for Reporting of Phase Equilibrium Measurements (IUPAC Recommendations 2012), Pure Appl. Chem. 84 (8) (2012) 1785–1813, URL http://dx.doi.org/10.1351/PAC-REC-11-05-02.

[17] BIPM, IEC, IFCC, ILAC, IUPAC, IUPAP, ISO, OIML, Evaluation of Measurement Data - Guide for the Expression of Uncertainty in Measurement. JCGM 100: 2008, 2008.

[18] S. F. Westman, H. G. J. Stang, S. Ø. Størset, H. Rekstad, A. Austegard, S. W. Løvseth, Accurate Phase Equilibrium Measurements of CO_2 Mixtures, 7th Trondheim Conference on CO_2 capture, Transport and Storage, June 2013, Energy Procedia 51 (2014) 392–401, URL http://dx.doi.org/10.1016/j.egypro.2014.07.046.

[19] M. E. Wieser, T. B. Coplen, Atomic weights of the elements 2009 (IUPAC Technical Report), Pure Appl. Chem. 83 (2) (2010) 359–396, URL http://dx.doi.org/10.1351/PAC-REP-10-09-14.

[20] M. E. Wieser, N. Holden, T. B. Coplen, J. K. Böhlke, M. Berglund, W. A. Brand, P. De Bièvre, M. Gröning, R. D. Loss, J. Meija, T. Hirata, T. Prohaska, R. Schoenberg, G. O'Connor, T. Walczyk, S. Yoneda, X.-K. Zhu, Atomic weights of the elements 2011 (IUPAC Technical Report), Pure Appl. Chem. 85 (5) (2013) 1047–1078, URL http://dx.doi.org/10.1351/PAC-REP-13-03-02.

[21] K. A. Essenhigh, Y. G. Utkin, C. Bernard, I. V. Adamovich, J. W. Rich, Gas-phase Boudouard disproportionation reaction between highly vibrationally excited CO molecules, Chem. Phys. 330 (3) (2006) 506–514, ISSN 0301-0104, URL http://dx.doi.org/10.1016/j.chemphys.2006.09.033.

[22] J. Brynestad, Iron and nickel carbonyl formation in steel pipes and its prevention: Literature survey, Tech. Rep., Oak Ridge National Lab., Tennesse, USA, 1976.

[23] P. Andersen, G. Cooper, The cylinder's impact on metal impurities in CO., Semiconductor International 21 (4) (1998) 127–129.

[24] B. D. Craig, D. S. Anderson, Handbook of Corrosion Data, ASM International, Materials Park, Ohio, USA, 2 edn., 1995.

[25] R. C. Shores, F. Smith, D. J. von Lehmden, Stability evaluation of sulfur dioxide, nitric oxide and carbon monoxide gases in cylinders, EPA/600/4-84/086 (NTIS PB85122646), Tech. Rep., U.S. Environmental Protection Agency, Research Triangle Park, North Carolina, USA, URL https://nepis.epa.gov/Exe/ZyPURL.cgi?Dockey=400011JF.txt, 1984.

[26] R. E. Walpole, R. H. Myers, S. L. Myers, K. Ye, Probability and statistics for engineers and scientists, 8th Ed., Pearson, ISBN 0132047675, 2007.

[27] R. Span, W. Wagner, A New Equation of State for Carbon Dioxide Covering the Fluid Region from the Triple-Point Temperature to 1100 K at Pressures up to 800 MPa, J. Phys. Chem. Ref. Data 25 (1996) 1509, URL http://dx.doi.org/10.1063/1.555991.

[28] G.-I. Kaminishi, Y. Arai, S. Saito, S. Maeda, Vapor-liquid equilibria for binary and ternary systems containing carbon dioxide, J. Chem. Eng. Jpn. 1 (2) (1968) 109–116, URL http://dx.doi.org/10.1252/jcej.1.109.

[29] S. T. Blanco, C. Rivas, R. Bravo, J. Fernández, M. Artal, I. Velasco, Discussion of the Influence of CO and CH_4 in CO2 Transport, Injection, and Storage for CCS Technology, Environ. Sci. Technol. 48 (18) (2014) 10984–10992, URL http://dx.doi.org/10.1021/es502306k.

[30] L. J. Christiansen, A. Fredenslund, N. Gardner, Gas-Liquid Equilibria of the CO_2–CO and CO_2–CH_4–CO Systems, Springer US, Boston, MA, ISBN 978-1-4613-9847-9, 309–319, URL http://dx.doi.org/10.1007/978-1-4613-9847-9_38, 1974.

[31] J. Ke, B. Han, M. W. George, H. Yan, M. Poliakoff, How Does the Critical Point Change during a Chemical Reaction in Supercritical Fluids? A Study of the Hydroformylation of Propene in Supercritical CO_2, J. Am. Chem. Soc. 123 (16) (2001) 3661–3670, URL http://dx.doi.org/10.1021/ja003446o.

[32] D. Köpke, Verfahrenstechnik der CO_2-Abscheidung aus CO_2-reichen Oxyfuel-Rauchgasen, PhD dissertation, Technische Universität Hamburg-Harburg, Hamburg, ISBN: 3-86853-950-6, URL https://www.tuhh.de/alt/fsp-energieumwelt/publications/phd-theses.html, 2010.

[33] P. Ungerer, B. Tavitian, A. Boutin, Applications of Molecular Simula-

This is the accepted version of an article published in Fluid Phase Equilibria
https://doi.org/10.1016/j.fluid.2018.05.006

tion in the Oil and Gas Industry. Monte Carlo Methods, chap. 2, Editions Technip, Paris, France, note: Equation 2.100 is lacking the critical composition term, 2005.
[34] V. Lachet, T. de Bruin, P. Ungerer, C. Coquelet, A. Valtz, V. Hasanov, F. Lockwood, D. Richon, Thermodynamic behavior of the CO_2+SO_2 mixture: Experimental and Monte Carlo simulation studies, Energy Procedia 1 (1) (2009) 1641 – 1647, URL http://dx.doi.org/10.1016/j.egypro.2009.01.215.
[35] J. Sengers, J. Levelt Sengers, A universal representation of the thermodynamic properties of fluids in the critical region, Int. J. Thermophys. 5 (2) (1984) 195–208, ISSN 0195-928X, URL http://dx.doi.org/10.1007/BF00505500.
[36] Ø. Wilhelmsen, A. Aasen, G. Skaugen, P. Aursand, A. Austegard, E. Aursand, M. A. Gjennestad, H. Lund, G. Linga, M. Hammer, Thermodynamic Modeling with Equations of State: Present Challenges with Established Methods, Ind. Eng. Chem. Res. 56 (13) (2017) 3503–3515, URL http://dx.doi.org/10.1021/acs.iecr.7b00317.
[37] D.-Y. Peng, D. B. Robinson, A New Two-Constant Equation of State, Ind. Eng. Chem. Fundam. 15 (1) (1976) 59–64, URL http://dx.doi.org/10.1021/i160057a011.
[38] P. M. Mathias, T. W. Copeman, Extension of the Peng-Robinson equation of state to complex mixtures: Evaluation of the various forms of the local composition concept, Fluid Phase Equilib. 13 (1983) 91–108, URL http://dx.doi.org/10.1016/0378-3812(83)80084-3.
[39] D. S. H. Wong, S. I. Sandler, A Theoretically Correct Mixing Rule for Cubic Equations of State, AIChE J. 38 (5) (1992) 671–680, URL http://dx.doi.org/10.1002/aic.690380505.
[40] H. Renon, J. M. Prausnitz, Local compositions in thermodynamic excess functions for liquid mixtures, AIChE J. 14 (1) (1968) 135–144, URL http://dx.doi.org/10.1002/aic.690140124.
[41] C. Coquelet, A. Valtz, F. Dieu, D. Richon, P. Arpentinier, F. Lockwood, Isothermal P, x, y data for the argon+carbon dioxide system at six temperatures from 233.32 to 299.21 K and pressures up to 14 MPa, Fluid Phase Equilib. 273 (1-2) (2008) 38–43, URL http://dx.doi.org/10.1016/j.fluid.2008.08.010.
[42] P. T. Boggs, R. H. Byrd, J. E. Rogers, R. B. Schnabel, User's Reference Guide for ODRPACK Version 2.01 Software for Weighted Orthogonal Distance Regression, URL http://docs.scipy.org/doc/external/odrpack_guide.pdf, 1992.
[43] O. Chiavone-Filho, P. G. Amaral Filho, D. N. Silva, L. R. Terron, Alpha Function for a Series of Hydrocarbons to Peng-Robinson and van der Waals Equations of State, Ind. Eng. Chem. Res. 40 (26) (2001) 6240–6244, URL http://dx.doi.org/10.1021/ie001134o.
[44] E. W. Lemmon, R. Span, Short Fundamental Equations of State for 20 Industrial Fluids, J. Chem. Eng. Data 51 (3) (2006) 785–850, URL http://dx.doi.org/10.1021/je050186n.
[45] R. D. Goodwin, Carbon Monoxide Thermophysical Properties from 68 to 1000 K at Pressures to 100 MPa, J. Phys. Chem. Ref. Data 14 (4) (1985) 849–932, URL http://dx.doi.org/10.1063/1.555742.

This is the accepted version of an article published in Fluid Phase Equilibria
https://doi.org/10.1016/j.fluid.2018.05.006